



## Reversible dioxygen binding and arene hydroxylation reactions: Kinetic and thermodynamic studies involving ligand electronic and structural variations

Kenneth D. Karlin<sup>a,\*</sup>, Christiana Xin Zhang<sup>a</sup>, Arnold L. Rheingold<sup>b</sup>, Benedikt Galliker<sup>c</sup>, Susan Kaderli<sup>c</sup>, Andreas D. Zuberbühler<sup>c,\*</sup>

<sup>a</sup> Department of Chemistry, The Johns Hopkins University, Baltimore, MD 21218, USA

<sup>b</sup> Department of Chemistry, University of Delaware, Newark, DE 19716, USA

<sup>c</sup> Department of Chemistry, University of Basel, 4056 Basel, Switzerland

### ARTICLE INFO

#### Article history:

Available online 2 February 2012

Dedicated to Professor Jon Zubieta on the occasion of his 65th birthday. All the best to a special guy and wonderful colleague who without hesitation or reservation significantly influenced and aided the launching of K.D.K.'s research career. One could not be more grateful

#### Keywords:

Copper–dioxygen complexes

Peroxo

Hydroxylation

O<sub>2</sub>-activation

Kinetics–thermodynamics

### ABSTRACT

Copper–dioxygen interactions are of intrinsic importance in a wide range of biological and industrial processes. Here, we present detailed kinetic/thermodynamic studies on the O<sub>2</sub>-binding and arene hydroxylation reactions of a series of xylyl-bridged binuclear copper(I) complexes, where the effects of ligand electronic and structural elements on these reactions are investigated. Ligand 4-pyridyl substituents influence the reversible formation of side-on bound  $\mu$ - $\eta^2$ : $\eta^2$ -peroxodicopper(II) complexes, with stronger donors leading to more rapid formation and greater thermodynamic stability of product complexes  $[\text{Cu}^{\text{II}}_2(\text{RXYL})(\text{O}_2^{2-})]^{2+}$ . An interaction of the latter with the xylyl  $\pi$ -system is indicated. Subsequent peroxo electrophilic attack on the arene leads to C–H activation and oxygenation with hydroxylated products  $[\text{Cu}^{\text{II}}_2(\text{RXYLO})(\text{OH})]^{2+}$  being formed. A related unsymmetrical binucleating ligand was also employed. Its corresponding O<sub>2</sub>-adduct  $[\text{Cu}^{\text{II}}_2(\text{UN})(\text{O}_2^{2-})]^{2+}$  is more stable, but primarily because the subsequent decay by hydroxylation is in a relative sense slower. The study emphasizes how ligand electronic effects can and do influence and tune copper(I)–dioxygen complex formation and subsequent reactivity.

© 2012 Elsevier B.V. All rights reserved.

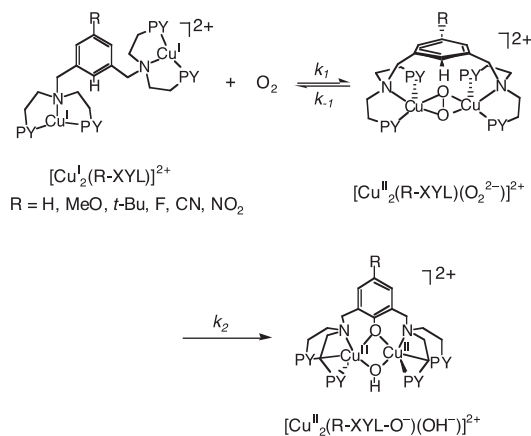
### 1. Introduction

Interests in copper(I)–dioxygen reactivity of coordination complexes derive from the need to establish fundamental properties and due to the occurrence of such chemistry in a variety of copper proteins which are essential in O<sub>2</sub>-processing in aerobic organisms [1]. Notable examples of the latter include hemocyanins [2] (dioxygen carriers in arthropods and mollusks) and enzymes involved in O<sub>2</sub>-activation towards substrate oxidations such as tyrosinase (Tyr) [3], dopamine  $\beta$ -monooxygenase (D $\beta$ M) [4], peptidyl  $\alpha$ -amidating monooxygenase (PHM) [4] and particulate (membrane bound) copper-dependent methane monooxygenase (pMMO) [1c,5]. The monooxygenase Tyr employs a coupled binuclear copper site similar to that in hemocyanin, where the reduced dicopper(I) site reacts with O<sub>2</sub> giving a side-on (or  $\mu$ - $\eta^2$ : $\eta^2$ ) peroxodicopper(II) species capable of phenol oxygenation, producing *o*-catechol or *o*-quinone directly.

With aromatic ring hydroxylation via Cu<sup>I</sup>/O<sub>2</sub> chemistry as a goal in Tyr modeling, we earlier on discovered and detailed the chemis-

try with a binuclear copper(I) complex  $[\text{Cu}^{\text{I}}_2(\text{H-XYL})]^{2+}$  which quantitatively reacts with resulting in the hydroxylation of the 2-position of the arene spacer (Scheme 1) [6]. A Cu<sub>2</sub>O<sub>2</sub> reactive intermediate,  $[\text{Cu}_2(\text{XYL})(\text{O}_2^{2-})]^{2+}$  (Scheme 1) with a side-on bridging peroxide moiety similar to that for oxy-hemocyanin and oxy-tyrosinase was proven based on its UV–Vis spectroscopic features ( $\lambda_{\text{max}} = 360, 435 \text{ nm}$ ) and resonance Raman (rR) spectroscopic properties (for R = NO<sub>2</sub>) [6b,c]. The reaction mechanism deduced for this hydroxylation chemistry involves an electrophilic attack of the arene by the side-on peroxo moiety. Theoretical studies supported this conclusion [6b], however this was first shown by substituent effect studies where for R = MeO, *t*-Bu, F, CN, and NO<sub>2</sub> at the 5-position of the arene (Scheme 1), the rate constants ( $k_2$ ) for arene hydroxylation increased with R electron-donating ability [6c,7]. Further support for the electrophilic mechanism came from studies where a 2-Me substituted xylyl ligand was employed, as a hydroxylation-induced methyl-migration (i.e. “N.I.H.” shift) occurred [8]. As an interesting aside, a substituent effect on the dioxygen binding to  $[\text{Cu}^{\text{I}}_2(\text{R-XYL})]^{2+}$  where electron donating R-groups increased the copper–dioxygen binding strength was rationalized by the suggestion that an interaction between the xylyl  $\pi$ -system and the peroxo group occurs [6b,7].

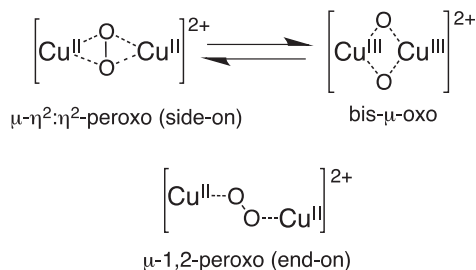
\* Corresponding authors. Tel.: +1 4015168027; fax: +1 4105167044 (K.D. Karlin).  
E-mail address: [karlin@jhu.edu](mailto:karlin@jhu.edu) (K.D. Karlin).



**Scheme 1.** Dicopper mediated hydroxylation of arenes as copper monooxygenase models systems.

While a good number of other binuclear copper(I) complexes with *m*-xylyl linker were since shown to also exhibit arene hydroxylation chemistry [9], considerable attention has also focused on dicopper systems effecting phenol *o*-hydroxylation. In this context, elegant studies by Itoh and coworkers [3b] revealed that such chemistry occurs efficiently, not only with certain pyridylalkylamine chelates in synthetic models, but also with the enzyme Tyr itself. In both cases, the reactive intermediate is a  $[\text{Cu}_2^{\text{II}}(\mu\text{-}\eta^2\text{:}\eta^2\text{-O}_2^{2-})]^{2+}$  species which attacks the phenol substrate as an electrophile in a manner very similar to that of our  $[\text{Cu}_2(\text{XYL})]^{2+}$  system (Scheme 1). Yet, the Tolman and Stack research groups showed that  $\text{Cu}^{\text{II}}_2(\mu\text{-}\eta^2\text{:}\eta^2\text{-O}_2^{2-})$  are often in equilibrium with an isomeric bis- $\mu$ -oxo dicopper(III)  $[\text{Cu}^{\text{III}}_2(\text{O})_2]^{2+}$  species (Scheme 2) [1d,e,10] and it has been shown that these groups have also shown the latter to be capable of arene and *o*-phenol hydroxylation [1d,e,9b,10b]. As a relevant aside for the studies described above for the oxygenation of  $[\text{Cu}_2(\text{R-XYL})]^{2+}$  complexes, the side-on peroxo complex intermediate was readily detected and characterized, while no hint of a related bis- $\mu$ -oxo species  $[\text{Cu}^{\text{III}}_2(\text{NO}_2\text{-XYL})(\text{O})_2]^{2+}$  was found experimentally; this and theoretical studies support only the side-on peroxo-dicopper(II) species as the reacting electrophile in the  $\text{Cu}_2(\text{XYL})$  hydroxylation system [6b]. Computational studies on Tyr itself lead to a variety of conclusions. Thus, while a bis- $\mu$ -oxo-dicopper(III) entity has never been detected in Tyr, the chemical model studies leave the possibility of an unobservable enzyme  $[\text{Cu}^{\text{II}}_2(\mu\text{-}\eta^2\text{:}\eta^2\text{-O}_2^{2-})]^{2+}$  to  $[\text{Cu}^{\text{III}}_2(\text{O})_2]^{2+}$  conversion induced by phenol/phenolate substrate copper coordinations [10b,11].

To further elucidate fundamental aspects of the XYL type dicopper(I)/ $\text{O}_2$  chemistry involving both  $\text{O}_2$ -complex formation and substrate hydroxylation, we have here extended our kinetic-thermodynamic studies on the oxygenation reactions of a related but new series of complexes focusing on the influence of ligand



**Scheme 2.** Structures of well established dicopper  $\text{O}_2$ -adducts.

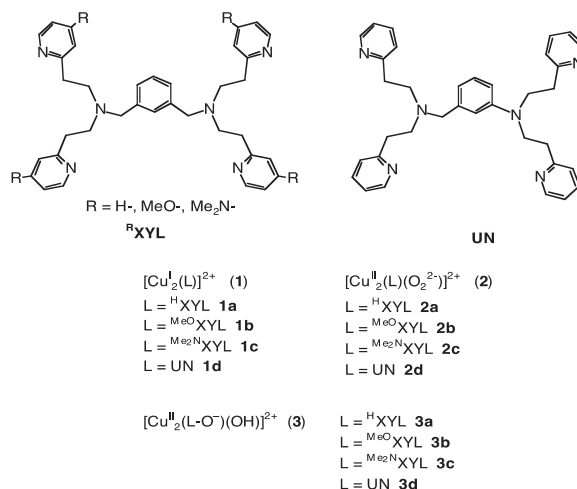


**Fig. 1.** Ligands used in this study of copper-dioxygen kinetics.

electronic and structural elements. Investigations of variations in ligand electron-donating ability in  $\text{Cu}^{\text{I}}/\text{O}_2$  chemistry have in the past been extremely revealing [7,12], also see the discussion below. Here, this is achieved by incorporating various 4-pyridyl substituents into the XYL ligands. An unsymmetrical ligand analogue UN (Fig. 1) is utilized to investigate the effect of ligand constraints on the  $\text{O}_2$ -interaction of the resulting dicopper(I) complex.

## 2. Experimental

### 2.1. Material and methods

Reagents and solvents used were of commercially available reagent quality unless otherwise stated. Methylene chloride and diethyl ether were purified by passing through an alumina column under Ar. Preparation and handling of air-sensitive materials were carried out under an argon atmosphere by using standard Schlenk techniques. Deoxygenation of solvents and solutions was achieved by bubbling with Ar for  $\sim 1/2$  h or by three freeze/pump/thaw cycles. Solid samples were stored and transferred in an MBraun drybox filled with prepurified nitrogen. Samples for IR, NMR and UV spectra were also prepared in the drybox.

$^1\text{H}$  NMR spectra were recorded in  $\text{CD}_3\text{NO}_2$ , or  $\text{CDCl}_3$  on a Bruker AMX-300 NMR spectrometer. Chemical shifts are reported as  $\delta$  values downfield from an internal TMS reference. Elemental analyses were performed by Desert Analytics, Tucson, AZ. EI/CI and FAB Mass spectra were obtained on a VG Instruments 70S Gas Chromatography/Mass Spectrometer by Dr. J. Kachinzki, Mass Spectrometry Facility, Department of Chemistry, the Johns Hopkins University. Infrared spectra were recorded as Nujol mulls on a Mattson Galaxy 4030 series FT-IR spectrophotometer and calibrated with a polystyrene film. UV-Vis spectra were collected on Hewlett-Packard Model 8453 diode array spectrophotometer with HP Chemstation software.

### 2.2. Syntheses of ligands and copper(I) complexes

#### 2.2.1. $\text{MeOXYL}$

To 4-methoxy-2-vinylpyridine (1.6 g, 0.012 mol) in a 15 mL pressure tube (Aldrich) was added *m*-xylenediamine (0.35 g, 0.0025 mol) and MeOH (2 mL) along with five drops of glacial acetic acid. The resulting mixture was stirred at 60 °C for 5 days. After cooling to room temperature, the volatile components were removed by rotary evaporation. The residual acetic acid was neutralized with  $\text{Na}_2\text{CO}_3$  aqueous solution. The resulting solution was extracted with  $\text{CH}_2\text{Cl}_2$  three times. The combined organic extracts

were dried over  $\text{Na}_2\text{SO}_4$  and the volatile components were removed by rotary evaporation. Purification of the crude product on alumina gel using 5% MeOH–95% EtOAc gave 1.1 g (64%) of yellow oil.  $R_f = 0.4$  (silica, 10% MeOH–90% EtOAc).  $^1\text{H NMR}$  (300 MHz,  $\text{CDCl}_3$ ):  $\delta$  8.27 (4H, d,  $J = 6.0$  Hz), 7.16–7.07 (4H, m), 6.63–6.50 (8H, m), 3.76 (12H, s), 3.67 (4H, s), 2.93 (16H, m). FAB-MS ( $m/z$ ): 677 ( $\text{M}+\text{H}^+$ ).

### 2.2.2. $\text{Me}^{2\text{N}}\text{XYL}$

To 4-dimethylamino-2-vinylpyridine (3.2 g, 0.022 mol) in a 15 mL pressure tube (Aldrich) were added *m*-xylenediamine (0.70 g, 0.0051 mol) and MeOH (10 mL) along with glacial acetic acid (0.63 g, 0.011 mol). The resulting mixture was stirred at 60 °C for 5 days. After cooling to room temperature, the volatile components were removed by rotary evaporation. The residual acetic acid was neutralized with  $\text{Na}_2\text{CO}_3$  aqueous solution. The resulting solution was extracted with  $\text{CH}_2\text{Cl}_2$  three times. The combined organic extracts were dried over  $\text{Na}_2\text{SO}_4$  and the volatile components were removed by rotary evaporation. Purification of the crude product on alumina gel using 3% MeOH–97% EtOAc gave 1.0 g (27%) of yellow oil.  $R_f = 0.19$  (silica, 3%  $\text{NH}_4\text{OH}$ , 97% MeOH).  $^1\text{H NMR}$  (300 MHz,  $\text{CDCl}_3$ ):  $\delta$  8.11 (4H, d,  $J = 6.0$  Hz), 7.23–7.12 (4H, m), 6.31–6.29 (8H, m), 3.71 (4H, s), 2.93–2.82 (40H, m). FAB-MS ( $m/z$ ): 729.6 ( $\text{M}+\text{H}^+$ ).

### 2.2.3. $[\text{Cu}^{\text{I}}(\text{MeOXYL})](\text{PF}_6)_2$ (**1b**)

Under an Ar atmosphere, 0.297 g (0.439 mmol) of  $\text{MeOXYL}$  in 20 mL of  $\text{CH}_2\text{Cl}_2$  was deaerated for 20 min and then added to 0.320 g (0.859 mmol) of  $[\text{Cu}(\text{CH}_3\text{CN})_4](\text{PF}_6)_2^{28}$  in a 100 mL Schlenk flask. The resulting solution was stirred for ½ h and then cooled to –78 °C. Addition of 100 mL of deaerated diethyl ether precipitated out light yellow powder. After warming to room temperature, the solvent was decanted and the solid was washed with  $\text{CH}_2\text{Cl}_2$ /diethyl ether (v:v, 1:5) for five times. The solid was dried under vacuum to afford 0.25 g (27%) of light yellow powder.  $^1\text{H NMR}$  (300 MHz,  $\text{CD}_3\text{NO}_2$ ):  $\delta$  8.30 (4H, d), 7.43 (1H, s), 7.09–7.22 (3H, m), 6.85–6.90 (8H, m), 3.92 (12H, s), 3.72 (4H, s), 3.11 (16H, s, br). *Anal. Calc.* for  $\text{C}_{40}\text{H}_{48}\text{N}_6\text{O}_4\text{F}_{12}\text{P}_2\text{Cu}_2$ : C, 43.92; H, 4.42; N, 7.68. Found: C, 43.92; H, 4.61; N, 7.97%.

### 2.2.4. $[\text{Cu}^{\text{I}}(\text{Me}^{2\text{N}}\text{XYL})](\text{PF}_6)_2 \cdot 1.1\text{CH}_2\text{Cl}_2$ (**1c**)

Under an Ar atmosphere, 0.213 g (0.292 mmol) of  $\text{Me}^{2\text{N}}\text{XYL}$  in 15 mL of MeOH was deaerated for 20 min and then added to 0.210 g (0.563 mmol) of  $[\text{Cu}(\text{CH}_3\text{CN})_4](\text{PF}_6)_2$  in a 100 mL Schlenk flask at 0 °C. The resulting mixture was stirred for 20 min and 70 mL of deaerated diethyl ether was added to precipitate out yellow powder. After decanting the solvent, the solid was redissolved in 20 mL of deaerated  $\text{CH}_2\text{Cl}_2$  at 0 °C and layered with 80 mL of diethyl ether to afford a yellow precipitate. The solvent was decanted and the solid was dried under vacuum for 2 h to yield 140 mg (44%) of yellow powder.  $^1\text{H NMR}$  (300 MHz,  $\text{CD}_3\text{NO}_2$ ):  $\delta$  8.03 (4H, d), 7.48 (1H, s), 7.11 (3H, m), 6.5 (8H, s), 5.32 (2.2H, s), 3.57 (4H, s), 3.11–3.04 (40H, m). *Anal. Calc.* for  $\text{C}_{44}\text{H}_{60}\text{N}_{10}\text{F}_{12}\text{P}_2\text{Cu}_2 \cdot 1.1\text{CH}_2\text{Cl}_2$ : C, 43.5; H, 5.04; N, 11.22. Found: C, 43.2; H, 5.14; N, 11.22%.

### 2.2.5. $[\text{Cu}^{\text{II}}(\text{MeOXYLO}^-)(\text{OH}^-)](\text{PF}_6)_2 \cdot 0.5\text{CH}_2\text{Cl}_2$ (**3b**)

In a 100 mL Schlenk flask,  $[\text{Cu}^{\text{I}}(\text{MeOXYL})](\text{PF}_6)_2$  (100 mg, 0.0914 mmol) was dissolved in 50 mL deaerated DMF under an Ar atmosphere. The resulting yellow solution was cooled to 0 °C and exposed to an atmosphere of dry oxygen overnight. The solvent was removed on a high-vacuum rotary evaporator and the green residue obtained was recrystallized from  $\text{CH}_2\text{Cl}_2$ /ether at 0 °C, giving 95 mg (48%) of green crystalline solid. *Anal. Calc.* for  $\text{C}_{40}\text{H}_{48}\text{N}_6\text{Cu}_2\text{O}_6\text{P}_2\text{F}_{12} \cdot 0.5\text{CH}_2\text{Cl}_2$ : C, 41.64; H, 4.23; N, 7.19. Found: C, 41.81; H, 4.15; N, 7.20%.  $\mu_{\text{eff}}$  (Evans method,  $\text{CD}_2\text{Cl}_2$ ):

$1.08 \pm 0.10$  B.M. UV–Vis (nm,  $\text{CH}_2\text{Cl}_2$ ): 370 ( $\epsilon = 3450$ ), 637 ( $\epsilon = 150$ ). IR (nujol,  $\text{cm}^{-1}$ ): 3643 (br, OH), 840 (s,  $\text{PF}_6$ ). A  $^1\text{H NMR}$  spectrum of **3b** exhibits broad paramagnetically-shifted resonances and the presence of  $\text{CH}_2\text{Cl}_2$  solvate was indicated by a relatively sharp peak at 5.32 ppm.

### 2.3. Stopped-flow kinetics experiments

Rapid kinetics were followed using a SFL-21 (2-mm light path/2-mL syringes) low-temperature flow unit of a SF-3A stopped-flow system (Hi-Tech Scientific) combined with a TIDAS-16 HQ/UV–Vis 512/16B diode array spectrometer (J & M, 507 diodes, 300–720 nm, 1.3 ms minimum sampling time) using flexible light guides connected to a CLH-111 halogen lamp (ZEISS). The two glass coils, containing Cu(I) and oxygen solutions, respectively, and the mixing chamber, were immersed in an ethanol bath. This bath was placed in a dewar, which was filled with liquid nitrogen for low-temperature measurements. The ethanol bath was cooled by liquid nitrogen evaporation, and its temperature was measured by using a Pt resistance thermometer and maintained to 0.1 °C by using a temperature-controlled thyristor power unit (both Hi-Tech).

Data acquisition (up to 256 complete spectra, up to four different time bases) was done based on the KINSPEC program (J & M). For numerical analysis, all data were pretreated by factor analysis and concentration profiles were calculated by numerical integration using either Specfit (Spectrum Software Ass.) or Globfit (MATLAB).

The solvent  $\text{CH}_2\text{Cl}_2$  (Uvasol, Merck) was dried with  $\text{CaH}_2$  (Merck) and distilled under normal pressure immediately prior to use. For  $[\text{Cu}_2^{\text{I}}(\text{Me}^{2\text{N}}\text{XYL})](\text{PF}_6)_2$  seven series of Cu(I) concentrations were used to carry out a total of 365 measurements between –90 and +20 °C. Of these 257 were used for the final analysis. The concentrations of Cu(I) solutions used were: 0.10, 0.17, 0.21, 0.37 mM (with a dioxygen concentration of 1.90 mM); 0.13 mM ( $[\text{O}_2] = 0.50$  mM); 0.24 mM ( $[\text{O}_2] = 0.24$  mM) and 0.12 mM ( $[\text{O}_2] = 0.13$  mM). Reaction times measured ranged from 0.02 to 158 s.

For  $[\text{Cu}_2^{\text{I}}(\text{UN})](\text{PF}_6)_2$  nine series of Cu(I) concentrations were used to carry out a total of 222 measurements between –90 and –35 °C. Two hundred and eighteen of these were used for the final analysis. For one series, a cutoff filter (480 nm) was used. The concentrations of Cu(I) solutions used varied between 0.14 and 1.08 mM. The dioxygen concentrations varied between 0.25 and 1.9 mM. Reaction times measured ranged from 172 to 227 s.

For  $[\text{Cu}_2^{\text{I}}(\text{MeOXYL})](\text{PF}_6)_2$ , three series of Cu(I) concentrations were used to carry out a total of 91 measurements between –91 and +20 °C. Seventy-two of these were used for the final analysis. The concentrations of Cu(I) solutions used were 0.15, 0.30 and 0.41 mM. The dioxygen concentration used throughout was 1.9 mM. Reaction times measured ranged from 4 to 301 s.

### 2.4. Electrochemistry

Cyclic voltammetry was carried out by using a Bioanalytical Systems BAS-100B Electrochemistry Analyzer. The cell consisted of a modification of a standard three-chamber design equipped for handling air-sensitive solution by utilizing high-vacuum valve seals. A platinum disk (BAS MF 2013) was used as the working electrode. The reference electrode was Ag/AgNO<sub>3</sub>. The measurements were performed at room temperature under an Ar atmosphere in DMF solution containing 0.2 M tetrabutylammonium hexafluorophosphate and  $10^{-4}$ – $10^{-3}$  M copper complex.

### 2.5. Magnetic moment measurements

Room temperature solution magnetic moments of the complex **3b** were determined using the Evans method [13]. NMR sample tubes with screw caps and coaxial insert were purchased from

the Wilmad Glass Company. Solutions of **3b** with known concentrations were placed in the NMR sample tube and the deuterated reference solvent along with a small drop of undeuterated solvent to facilitate the identification of the reference solvent peak in NMR spectra were placed in the coaxial insert. The  $^1\text{H}$  NMR spectra were taken on a Bruker AMX-300 NMR spectrometer. The chemical shift difference of the solvent was used to calculate the molar magnetic susceptibility of the complex based on the following equation:

$$c_M = (-3/4\pi)(Dn/n)(1000/c) + c_M^{\text{sol}} - c_D,$$

where  $Dn$  is the paramagnetic shift of the solvent as the product of the chemical shift difference  $Dd$  and  $n$  (frequency of the NMR spectrometer),  $c$  is the sample concentration,  $c_M^{\text{sol}}$  is the solvent susceptibility and  $c_D$  is the diamagnetic correction.  $c_M^{\text{sol}}$  can be calculated as the product of  $c_g$  (value obtained from the CRC hand book) and the molecular weight of the metal complex. The value of  $c_D$  is obtained based on the molecular formulation of the complex and Pascal's constants. The solution magnetic moment is related to the magnetic susceptibility as follows:  $\mu = 2.84((c_M T/n))^{1/2}$ , where  $n$  is the nuclearity.

### 2.6. Low-temperature UV–Vis spectroscopy

Low-temperature UV–Vis spectra were recorded on a Hewlett-Packard HP8453 diode array spectrophotometer using a custom manufactured vacuum dewar equipped with quartz windows. To maintain and control low temperatures, a copper-tubing coil was inserted into the methanol-filled UV–Vis dewar through which cold methanol was circulated from an external source (Neslab Endocal refrigerated circulating bath). The temperature in the dewar was monitored by using a resistance thermocouple probe (Omega Model 651). The cuvette assembly consists of a quartz cell with 2 mm pathlength connected to a 14/20 female joint via a 10-cm long glass tube. The apparatus and procedures have also been previously described [14].

A solution of the Cu(I)-complex **1b–d** with a known concentration was prepared in a glovebox and transferred into a cuvette with 2 mm pathlength. Then the cuvette was brought out of the glovebox and placed in the UV–Vis low-temperature (193 K) dewar. The UV–Vis spectrum of the copper(I) complex was recorded after 20 min. Then excess  $\text{O}_2$  was introduced to the Cu(I) solution through a syringe needle and spectrum of the  $\text{O}_2$ -adduct was recorded and monitored over time to determine its stability.

## 3. Results and discussion

### 3.1. Employing ligand 4-pyridyl substituents in $\text{Cu}^{\text{I}}/\text{O}_2$ reactivity studies

The use of 4-pyridyl substituents has already proven very useful in a number of studies involving copper–dioxygen complex formation and reactivity, demonstrating that they mediate changes in the kinetics and thermodynamics of  $\text{Cu}_2\text{O}_2$  complexes, the equilibria involving different structural isomers of  $\text{Cu}_2\text{O}_2$  species, and the subsequent reactivity of such complexes [7,12]. In a notable study [12a], we showed that for  $\{[(\text{R-TMPA})\text{Cu}^{\text{II}}]_2(\text{O}_2^{2-})\}^{2+}$  (Scheme 3), the observed  $\nu_{\text{O-O}}$  value shifts from 827 to 822 to  $812\text{ cm}^{-1}$  and  $\nu_{\text{Cu-O}}$  (sym) shifts from 561 to 557 to  $551\text{ cm}^{-1}$ , respectively, as R- varies from H- to MeO- to  $\text{Me}_2\text{N-}$ . Increasing the N-donor strength to the copper decreases peroxide  $\pi^*\sigma$  donation to the copper, weakening the Cu–O and O–O bonds. A decrease in  $\nu_{\text{Cu-O}}$  of the bis- $\mu$ -oxo-dicopper(III) complex was also observed with increasing N-donor strength for the R-MePY2 ligand system (Scheme 3). However, no change was observed for  $\nu_{\text{O-O}}$  of the side-on peroxo moiety which is attributed to a compensating reduced charge donation from the

peroxide  $\pi^*\sigma$  orbital (to Cu) with increased ligand N-donor strength; this increases the effective negative charge on the peroxide moiety and thus reduces the backbonding from the Cu to the peroxide  $\pi^*$  orbital. However, an increase in the amount of bis- $\mu$ -oxo-dicopper(III) isomer relative to side-on peroxo-dicopper(II) species is observed for R-MePY2 with  $\text{R} = \text{H} < \text{MeO} < \text{Me}_2\text{N}$ . The stronger donor ligands increase the stability of the  $\text{Cu}^{\text{III}}(\mu\text{-O})_2$  isomer with its higher oxidation state metal ion. In a related study [15], copper ion complexes of so-called PYAN ligands (R-PYAN =  $N$ -[2-(4-R-pyridin-2-yl)-ethyl]- $N,N,N'$ -trimethyl-propane-1,3-diamine,  $\text{R} = \text{Cl-}, \text{H-}, \text{MeO-}$  and  $\text{Me}_2\text{N-}$ ) were even more severely influenced with respect to the side-on peroxo-dicopper(II)/bis- $\mu$ -oxo-dicopper(III) equilibrium. For  $\text{R} = \text{Cl-}$ , the  $\text{Cu}_2\text{O}_2$  species generated consisted entirely of the former isomer, while for  $\text{Me}_2\text{N-}$ , nearly entirely the latter.

We also studied the kinetic–thermodynamic behavior for the formation and stability of  $\{[(\text{R-TMPA})\text{Cu}^{\text{II}}]_2(\text{O}_2^{2-})\}^{2+}$  complexes [12b]. In EtCN, a strongly coordinating solvent, the ligand electronic effects were dampened due to the competitive binding of solvent and dioxygen to the copper centers, especially with weaker electron-donating groups such as Me and tBu, and there was little affect on kinetic and thermodynamic parameters for the formation of both the superoxocopper(II) species  $[(\text{R-TMPA})\text{Cu}^{\text{II}}(\text{O}_2^-)]^+$  intermediate first formed (not shown) and the final product  $\{[(\text{R-TMPA})\text{Cu}^{\text{II}}]_2(\text{O}_2^{2-})\}^{2+}$  species (Scheme 3). But with stronger MeO- and  $\text{Me}_2\text{N-}$  electron-donating groups, the rates of formation and stability of the product complexes were increased, as  $\text{O}_2$ -binding to copper(I) is a redox process, thus favored when oxidation of the metal ion is also preferred. Significant medium (solvent) effects were also seen, with the non-coordinating solvents THF or acetone. The rates of formation of both superoxo and peroxo complexes, along with their thermodynamic stabilities were much enhanced when stronger donor ligands such as MeO- or  $\text{Me}_2\text{N-}$  4-pyridyl substituents were employed.

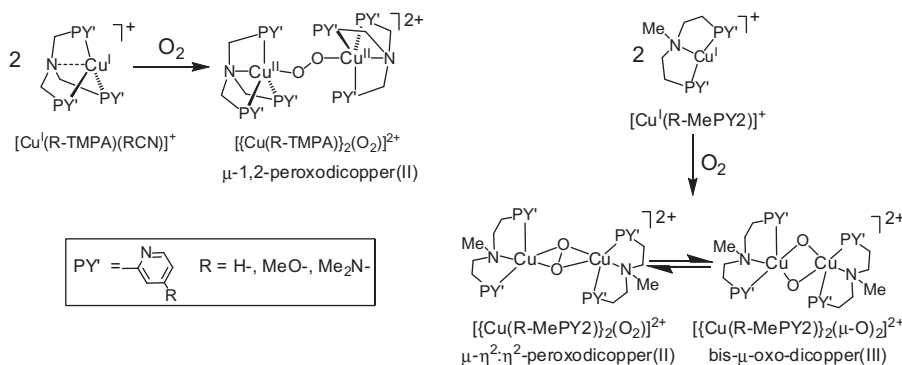
As mentioned above, the complexes  $\{[\text{Cu}(\text{R-MePY2})]_2(\text{O}_2)\}^{2+}$  possess a varying side-on-peroxo to bis- $\mu$ -oxo dicopper isomer ratio. In reactivity toward substituted anilines (Scheme 4), oxidative N-dealkylation takes place, but the mechanism of reaction shifts as one goes from  $\text{R} = \text{H-}$  to  $\text{R} = \text{Me}_2\text{N-}$  [12d]. The former complex,  $\{[\text{Cu}(\text{H-MePY2})]_2(\text{O}_2)\}^{2+}$ , is a stronger one-electron oxidant and possesses a lesser amount of  $\text{Cu}^{\text{III}}_2(\mu\text{-O})_2$  species, the reaction appears to take place by a predominantly proton-coupled electron-transfer (PCET) or electron-transfer first/subsequent proton transfer (ETPT) mechanism. Hydrogen-atom transfer (HAT, or ET/PT) chemistry occurs for the  $\{[\text{Cu}(\text{Me}_2\text{N-MePY2})]_2(\text{O}_2)\}^{2+}$  species, a weaker oxidant with respect to one-electron ET, but perhaps better able to accommodate a H-atom transfer due to its possession of a more basic bridging oxo group, because of the stronger ligand donors.

### 3.2. Ligand syntheses

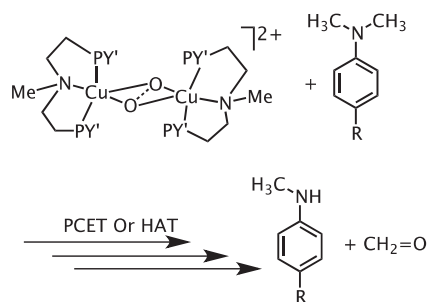
The ligand UN was prepared following a literature-based procedure [16], while  $^{\text{MeO}}\text{XYL}$  and  $^{\text{Me}_2\text{N}}\text{XYL}$  were synthesized in a similar manner through reactions of  $m$ -xylyldiamine with 4-substituted-2-vinylpyridines (Scheme 5); the latter syntheses are published [12a,c]. Also, see the Section 2 for details. As can be seen, the substituents chosen for new studies are  $\text{R} = \text{MeO-}$  and  $\text{Me}_2\text{N-}$ , strong donors compared to  $\text{R} = \text{H-}$  (Fig. 1). Electron-withdrawing groups were not included in these studies since we previously observed that for mononuclear Cu(I) complexes of in our studies on the Cl-MePY2 ( $\text{R} = \text{Cl-}$ ) (MePY2 =  $N$ -methyl- $N,N$ -bis[2-(2-pyridyl)ethyl]amine), there was no reaction with dioxygen [12c].

### 3.3. Synthesis of copper(I) complexes

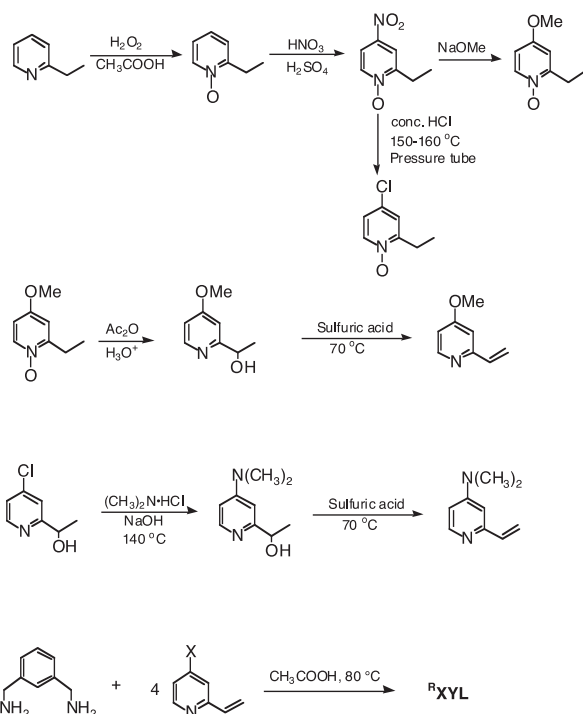
The dicopper(I) complexes  $[\text{Cu}_2(\text{L})]^{2+}$  (**1b–d**,  $\text{L} = ^{\text{MeO}}\text{XYL}, ^{\text{Me}_2\text{N}}\text{XYL}$  and UN, Fig. 1) were prepared by the addition of two equiv of



**Scheme 3.** Previously studied systems for copper(I)/O<sub>2</sub> kinetics employing derivatized pyridyl ligands.



**Scheme 4.** Cu<sub>2</sub>O<sub>2</sub> mediated oxidative N-dealkylation of dimethylanilines.



**Scheme 5.** Outline of the synthetic procedures to generate RXYL binucleating ligands.

[Cu'(MeCN)<sub>4</sub>](PF<sub>6</sub>) to the CH<sub>2</sub>Cl<sub>2</sub> solution of the appropriate ligand RXYL under an Ar atmosphere. Precipitation with diethyl ether followed by recrystallization affords light-yellow solids, which were characterized by <sup>1</sup>H NMR spectroscopy and elemental analyses. Repeated recrystallization from CH<sub>2</sub>Cl<sub>2</sub>/diethyl ether or

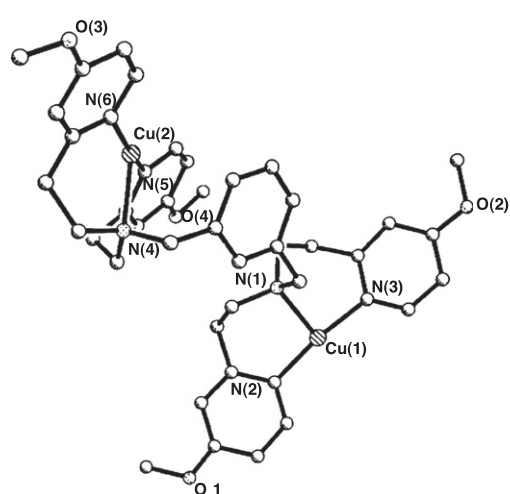


**Fig. 2.** Structure of the cationic portion of [Cu'<sub>2</sub>(<sup>MeO</sup>XYL)]<sup>2+</sup> (**1b**).

MeOH/diethyl ether was necessary for complete removal of MeCN (derived from [Cu'(MeCN)<sub>4</sub>](PF<sub>6</sub>)) as a coordinating fourth ligand to copper(I) ion with its tridentate N<sub>3</sub> chelate. This procedure led to the desired three-coordinate dicopper(I) complexes **1b–d** (Fig. 1).

### 3.4. X-ray structure of [Cu'<sub>2</sub>(<sup>MeO</sup>XYL)]<sup>2+</sup> (**1b**)

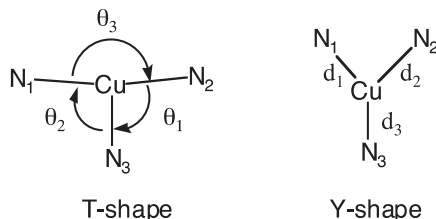
Light yellow crystals suitable for X-ray crystallography were obtained by slow diffusion of diethyl ether into an acetone solution of **1b**. The structure includes a *N,N*-dimethyl formamide (DMF) solvate molecule, possibly introduced as a solvent impurity. The cationic portion of the structure is shown in Fig. 2.

The structural parameters are similar to the previously reported dicopper(I) structure with the parent ligand <sup>H</sup>XYL (Table 1) [6a]. As shown in Fig. 1, each Cu(I) ion is three-coordinate with ligation from two pyridine nitrogens and one tertiary amine nitrogen donor. The chelating tridentate ligand causes considerable distortions from ideal trigonal planar coordination. The geometry of the copper centers can be best described as bent “T-shape” geometry. The N<sub>amino</sub>–Cu–N<sub>py</sub> (PY = 2-pyridyl) angles are acute within the range of 92–100°, resulting in large N<sub>py</sub>–Cu–N<sub>py</sub> angles of 163.9° and 166.5°. The Cu–N<sub>py</sub> bond distances (1.902–1.929 Å) in complex **1b** are typical for Cu–N<sub>heterocyclic</sub> (heterocyclic = derivatives of imidazole, pyrazole and pyridine) bond lengths in three-coordinate copper(I)-compounds [6a,17], and these short distances are approaching those found in purely linear two-coordinate systems with similar N-donor ligands, Cu–N ~ 1.86–1.89 Å [18]. The Cu–N<sub>amine</sub> distances are much longer than those of Cu–N<sub>py</sub>

**Table 1**  
Selected bond distances and angles for  $[\text{Cu}^{\text{I}}_2(\text{XYL})(\text{PF}_6)_2]$  (**1a**) and  $[\text{Cu}^{\text{I}}_2(\text{MeOXYL})(\text{PF}_6)_2]$  (**1b**) complexes.

$[\text{Cu}^{\text{I}}_2(\text{HXYL})(\text{PF}_6)_2]$ ( <b>1a</b> ) <sup>10</sup>				$[\text{Cu}^{\text{I}}_2(\text{MeOXYL})(\text{PF}_6)_2]$ ( <b>1b</b> )			
<i>Interatomic distances (Å)</i>							
Cu1–N1	2.121(8)	Cu1–N2	1.937(9)	Cu1–N1	2.289(7)	Cu1–N2	1.923(6)
Cu1–N3	1.924(8)	Cu2–N4	2.196(7)	Cu1–N31.917(6)	Cu2–N4	2.287(6)	
Cu2–N5	1.904(8)	Cu2–N6	1.918(8)	Cu2–N51.929(8)	Cu2–N6	1.902(8)	
<i>Interatomic angles (°)</i>							
N1–Cu1–N2	102.5(3)	N1–Cu1–N3	100.4(3)	N1–Cu1–N292.2(3)	N1–Cu1–N3	100.1(3)	
N2–Cu1–N3	151.4(4)	N4–Cu2–N5	99.7(3)	N2–Cu1–N3166.5(3)	N4–Cu2–N5	95.5(3)	
N4–Cu2–N6	104.4(3)	N5–Cu2–N6	150.8(3)	N4–Cu2–N699.2(3)	N5–Cu2–N6	163.9(3)	

distances, possibly due to the  $\pi$  back-donation (Cu(I) d electrons to the pyridine  $\pi^*$  orbitals). As shown in Table 1, the Cu–N<sub>amine</sub> distances in complex  $[\text{Cu}^{\text{I}}_2(\text{MeOXYL})(\text{PF}_6)_2]$  (**1b**) are longer by 0.1–0.2 Å than the corresponding bond lengths found in the parent complex  $[\text{Cu}^{\text{I}}_2(\text{XYL})(\text{PF}_6)_2]$  (**1a**) and the N<sub>PY</sub>–Cu–N<sub>PY</sub> angles are  $\sim 15^\circ$  larger than those found in the parent complex. This may be a ligand electronic effect, where greater electron density around the copper(I) centers resulting from the electron-donating 4-MeO- groups disfavors the coordination of  $\sigma$ -type ligands such as amine nitrogens (i.e., giving longer Cu–N<sub>amine</sub> distances). This results in larger N<sub>PY</sub>–Cu–N<sub>PY</sub> angles and more distortion from trigonal planar geometry.



Besides T-shaped copper(I) complexes, three-coordinate Y-shaped Cu(I)-complexes have also been described [19]. The bond angle  $\theta_3$  and the “middle” bond distance  $d_3$  increase as the geometry around the copper(I) distorts from the ideal trigonal planar geometry to T-shape, whereas both  $\theta_3$  and  $d_3$  decreases when the geometry moves from a trigonal planar to Y-shape geometry (see diagram).

### 3.5. Electrochemistry

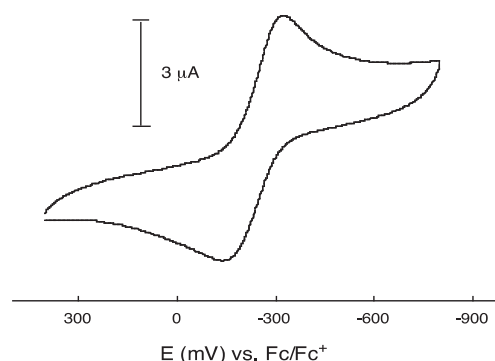
The redox potentials for the binuclear copper(I) complexes were measured by cyclic voltammetry (CV) under an Ar atmosphere in *N,N*-dimethylformamide (DMF) solution containing 0.2 M  $[\text{Bu}_4\text{N}][\text{PF}_6]$ . The potentials, listed in Table 2, are reported versus the ferrocene/ferrocenium couple. All the Cu(I)-complexes exhibit single quasi-reversible redox behavior with an  $i_{\text{pa}}/i_{\text{pc}}$  ratio close to unity. Fig. 2 shows a typical CV scan here for  $[\text{Cu}^{\text{I}}_2(\text{MeOXYL})(\text{PF}_6)_2]$  (**1b**) in DMF.

As shown in Table 2 and Fig. 3, only a single redox process is observed for these dicopper(I) complexes; no distinctive redox processes occur for the two Cu centers. A similar behavior was observed for analogous copper(I) complexes with either xylyl [20] or alkyl [20] linkers connecting two PY2 (=bis(2-(2-pyridyl)ethyl)amine) moieties. By contrast, differential pulse voltammetric measurements on bis(cyclam)dinickel and -dicopper complexes possessing variable methylene or xylyl linkers indicate that electrostatic effects and metal–metal distance as modified by linker length can influence the occurrence or extent of separation in CV experiments of the two metal-centered redox processes [21].

**Table 2**  
Cyclic voltammetry data for Cu(I)-complexes in DMF.<sup>a</sup>

Complex	$E_{1/2}$ (V)	$\Delta E_p$ (mV)	$i_{\text{pa}}/i_{\text{pc}}$
$[\text{Cu}^{\text{I}}_2(\text{HXYL})]^{2+}$ ( <b>1a</b> )	–0.21	210	0.95
$[\text{Cu}^{\text{I}}_2(\text{MeOXYL})]^{2+}$ ( <b>1b</b> )	–0.25	170	0.85
$[\text{Cu}^{\text{I}}_2(\text{NMe}_2\text{XYL})]^{2+}$ ( <b>1c</b> )	–0.28	300	1.15
$[\text{Cu}^{\text{I}}_2(\text{UN})]^{2+}$ ( <b>1d</b> )	–0.24	90	0.95

<sup>a</sup> Potentials are vs. Fc/Fc<sup>+</sup>, measured under the same electrochemical cell conditions.

**Fig. 3.** Cyclic voltammogram of  $[\text{Cu}^{\text{I}}_2(\text{MeOXYL})(\text{PF}_6)_2]$  (**1b**) in DMF.

As shown in Table 2, small redox potential shifts are observed as the ligands become more electron-donating; the  $E_{1/2}$  values become more negative as the R group goes from H- to MeO- to Me<sub>2</sub>N-. The observed ligand effect upon the redox potentials of the corresponding Cu(I)-complexes correlates to the differences in ligand basicity. The pK<sub>a</sub> values for pyridine, 4-MeO-pyridine and 4-Me<sub>2</sub>N-pyridine are 5.21, 6.58 and 9.70, respectively. The more basic ligand provides more electron density to the copper center, making it easier to oxidize Cu(I) to Cu(II). The same correlation between ligand basicity and the  $E_{1/2}$  values was observed for the mononuclear copper(I) analogues with 4-pyridyl substituted MePY2 ligands. However, more negative  $E_{1/2}$  values (–0.31 V for parent MePY2, –0.36 for MeO-MePY2 (with 4-MeO-pyridyl groups) and –0.44 for Me<sub>2</sub>N-MePY2 (with 4-Me<sub>2</sub>N-pyridyl groups)) are observed for the mononuclear copper(I) complexes compared to those for the corresponding dicopper(I) complexes. This may be due to the relative electron-donating capacities of the substituents on the central amine nitrogens, i.e. for the binuclear Cu(I)-complexes with xylyl linker, benzyl (PhCH<sub>2</sub>) groups are less electron-donating than Me- groups in the mononuclear copper(I) complexes  $[\text{Cu}^{\text{I}}(\text{R-MePY2})]^+$ , resulting in more positive redox potential for the binuclear complexes. However, a smaller shift (40 mV) was observed for the analogous mononuclear PhCH<sub>2</sub>-PY2 complex [22] where a Me- group is replaced with a PhCH<sub>2</sub>- group. Therefore, the observed more significant difference

in redox potentials for the binuclear Cu(I) complexes **1a–d** and the mononuclear Cu(I)-complexes  $[\text{Cu}^{\text{I}}(\text{R-MePY2})]^+$  may arise from some interaction between the two copper ions in the dicopper(I) complexes, where a nearby positively charged center makes the oxidation of one of the Cu(I) ions more difficult. In addition, relatively bigger shifts resulting from modifications in ligand electron-donating ability are observed for the mononuclear copper(I) complexes (130 mV shift from MePY2 to Me<sub>2</sub>N-MePY2 complexes) compared to those for the binuclear copper(I) complexes  $[\text{Cu}^{\text{I}}_2(\text{L})]^{2+}$  (**1a–c**) (70 mV shift from XYL to Me<sub>2</sub>NXYL complexes), described here, again suggesting possible interaction between the two copper centers in the binuclear complexes. In summary, it seems that the effect of ligand electron-donating ability on the redox potential of the metal ions in these binuclear complexes is reduced due to some (electrostatic) interaction between the two copper(I) centers.

A small negative shift in the  $E_{1/2}$  value is observed for  $[\text{Cu}^{\text{I}}_2(\text{UN})]^{2+}$  (**1d**) with the unsymmetrical ligand environment, compared to that for  $[\text{Cu}^{\text{I}}_2(\text{HXYL})]^{2+}$  (**1a**). Following the arguments made above, ligand constraints in UN may cause the copper ions to be held further apart, making it easier to oxidize Cu(I) to Cu(II) in complex.

Both ligand and structural properties are thus shown to affect the redox potentials of the corresponding copper(I) complexes. We previously observed that the difference in electrochemical behavior of copper(I) complexes with pyridyl and/or quinolyl ligands tended to correlate with variations in their O<sub>2</sub> reactivity [23]. The kinetic studies described below were carried out to investigate both ligand electronic and structural effects on the O<sub>2</sub>-interactions with the dicopper(I) complexes described here.

### 3.6. Isolation of the hydroxylation products

As previously described [6a,c,16], the oxygenation of  $[\text{Cu}^{\text{I}}_2(\text{XYL})](\text{PF}_6)_2$  and  $[\text{Cu}^{\text{I}}_2(\text{UN})](\text{PF}_6)_2$  in DMF at room temperature gives the corresponding phenoxo and hydroxo bridged dicopper(II) complexes  $[\text{Cu}^{\text{II}}_2(\text{XYLO}^-)(\text{OH})](\text{PF}_6)_2$  (**3a**) and  $[\text{Cu}^{\text{II}}_2(\text{UN-O}^-)(\text{OH})](\text{PF}_6)_2$  (**3d**). The stoichiometry of these reactions has been established by manometric measurements for O<sub>2</sub> uptake (Cu/O<sub>2</sub> = 2:1).<sup>10</sup> Mass spectrometric analysis of the oxygenated product of  $[\text{Cu}^{\text{I}}_2(\text{XYL})](\text{PF}_6)_2$  (**1a**) prepared by using isotopically pure <sup>18</sup>O<sub>2</sub> shows that both oxygen atoms in the  $[\text{Cu}^{\text{II}}_2(\text{XYLO}^-)(\text{OH})](\text{PF}_6)_2$  complex were incorporated into the final hydroxylation product.

Similarly, when the DMF solution of  $[\text{Cu}^{\text{I}}_2(\text{MeOXYL})](\text{PF}_6)_2$  (**1b**) was oxygenated at room temperature, a solution color change from yellow to dark green was observed. Isolation of the green complex yielded the hydroxylation product  $[\text{Cu}^{\text{II}}_2(\text{MeOXYLO}^-)(\text{OH})](\text{PF}_6)_2$  (**3b**) characterized by elemental analysis, X-ray crystallography, UV-Vis and IR spectroscopies, as well as room-temperature magnetic moment measurements. This complex exhibits UV-Vis features ( $\lambda_{\text{max}} = 370 \text{ nm}$  ( $\epsilon = 3450$ ),  $637 \text{ nm}$  ( $\epsilon = 150$ )), which are similar to those for complexes **3a** and **3d** [7,16]. The intense 370 nm absorption is assigned as an OH<sup>-</sup> → Cu(II) ligand-to-metal charge-transfer band and the weak absorption band at 637 nm is consistent with a *d-d* transition. The IR spectrum of complex **3b** exhibits a  $\nu_{\text{O-H}}$  at  $3643 \text{ cm}^{-1}$ . The room temperature magnetic moment of complex **3b** is  $1.1 \mu_{\text{B}}/\text{Cu}$ , comparable with  $0.8 \mu_{\text{B}}/\text{Cu}$  for **3a** [24], which indicates efficient antiferromagnetic coupling between the two Cu(II) centers through the bridging phenoxo and hydroxo ligands. Less efficient coupling is observed for the unsymmetrical complex  $[\text{Cu}^{\text{II}}_2(\text{UN-O}^-)(\text{OH})]^{2+}$  (**3d**) with a room temperature magnetic moment of  $1.5 \mu_{\text{B}}/\text{Cu}$  [16], manifesting the effect of ligand constraints in a distorted structure, where less efficient overlap of orbitals on the two separate Cu ions occurs. However, under synthetic conditions in CH<sub>2</sub>Cl<sub>2</sub> solvent, the hydroxylation reaction

seems to be least efficient for  $[\text{Cu}^{\text{I}}_2(\text{Me}_2\text{NXYL})]^{2+}$  (**1c**), where the unreacted ligand (approximately 40%) as well as the hydroxylated ligand were recovered after the oxygenation reaction. The lower hydroxylation efficiency in **1c** may arise from competition for an inter- rather than intra-molecular O<sub>2</sub>-binding process; this has previously been suggested in the oxygenation reactions of a series of analogous binuclear Cu(I)-complexes [7].

### 3.7. X-ray crystal structure of $[\text{Cu}^{\text{II}}_2(\text{MeOXYLO}^-)(\text{OH})](\text{PF}_6)_2$ (**3b**)

Green crystals suitable for X-ray crystallography were obtained by slow diffusion of diethyl ether into a methylene chloride solution of **3b**. Selected bond distances and angles are tabulated in Table 3, along with the corresponding structural parameters for the parent complex  $[\text{Cu}^{\text{II}}_2(\text{HXYLO}^-)(\text{OH})](\text{PF}_6)_2$  (**3a**) previously reported [6a] for comparison. An ORTEP view with atom labeling scheme is shown in Fig. 4.

Each copper ion is coordinated with three nitrogen atoms from the tridentate chelate along with the bridging-phenolate (O1) and hydroxide oxygen (O2) atoms in a slightly distorted square pyramidal geometry. The structural parameters are very similar to those of the parent complex, as shown in Table 3. The N3 and N5 pyridine nitrogen atoms occupy axial positions in an *anti* conformation with respect to the Cu<sub>2</sub>O<sub>2</sub> plane. These axially coordinated Cu-N<sub>py</sub> distances are 0.20 and 0.19 Å longer than those in the basal plane. The basal Cu-N<sub>py</sub> (N2 and N6) bond lengths average 1.99 Å, which are ca. 0.2 Å shorter than that in the parent complex  $[\text{Cu}^{\text{II}}_2(\text{XYLO}^-)(\text{OH})](\text{PF}_6)_2$  (**3a**) [6a], possibly due to the greater electron-donating abilities of the 4-MeO- compared to the unsubstituted pyridine nitrogen atoms.

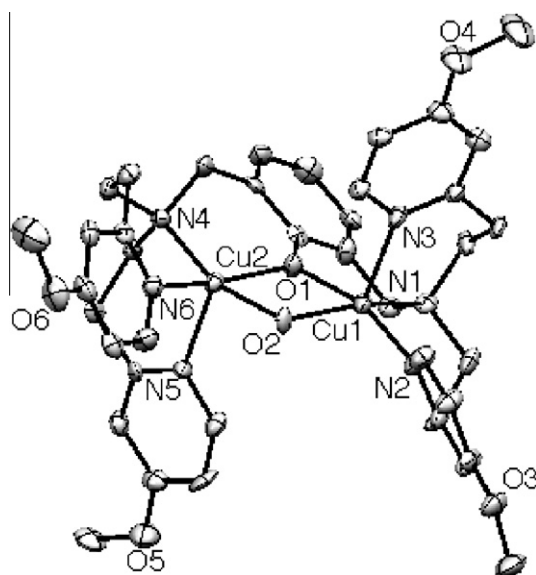
Similar to that in the parent complex, the Cu<sub>2</sub>O<sub>2</sub> unit is essentially planar and the phenolate ring is twisted with respect to the planar Cu<sub>2</sub>O<sub>2</sub> unit. The ligand orientation in these two complexes show substantial differences from the phenolate- and hydroxy-bridged binuclear Cu(II) complex with UN ligand, where the unsymmetrical ligand environment enforces the Cu<sub>2</sub>O<sub>2</sub> unit into a butterfly shape [16] and the two axial nitrogens engage in a *cis* conformation, in contrast to the *anti* conformation observed in the two symmetrical complexes (**3a** and **3b**). These structural differences have been shown to decrease the antiferromagnetic coupling between the two Cu(II) ions and to affect the O<sub>2</sub>-adduct formation and subsequent hydroxylation reactions, based on bench-top observations and kinetic measurements discussed below.

### 3.8. Bench-top oxygenation reactions in CH<sub>2</sub>Cl<sub>2</sub> at low temperature

When a bench-top low-temperature (193 K) oxygenation of  $[\text{Cu}^{\text{I}}_2(\text{HXYL})]^{2+}$  (**1a**) is carried out, no intermediate species  $[\text{Cu}^{\text{II}}_2(\text{HXYL})(\text{O}_2^{2-})]^{2+}$  could be observed spectroscopically. However, under the same conditions, the O<sub>2</sub>-adducts  $[\text{Cu}^{\text{II}}_2(\text{L})(\text{O}_2^{2-})]^{2+}$  (**2b–d**, L = MeOXYL, Me<sub>2</sub>NXYL, UN) with characteristic UV-Vis absorption features could be detected. The stability of  $[\text{Cu}^{\text{II}}_2(\text{MeOXYL})(\text{O}_2^{2-})]^{2+}$  (**2b**) and  $[\text{Cu}^{\text{II}}_2(\text{Me}_2\text{NXYL})(\text{O}_2^{2-})]^{2+}$  (**2c**) was still somewhat limited as indicated by the decrease in intensity of their characteristic electronic absorptions over time (~5 min). By contrast, the UN complex  $[\text{Cu}^{\text{II}}_2(\text{UN})(\text{O}_2^{2-})]^{2+}$  (**2d**) was much more stable at 193 K (no intensity decrease over 1 h) [16]. These bench-top observations manifest the ligand electronic or structural effects upon copper(I)-dioxygen adducts. However, rapid kinetic studies were needed to further understand, in a quantitative manner, how the ligand environment affects the O<sub>2</sub>-interactions of these dicopper(I) complexes (**1b–d**), followed by arene hydroxylation chemistry.

**Table 3**  
Selected bond distances and angles for **3c** and **1c**.

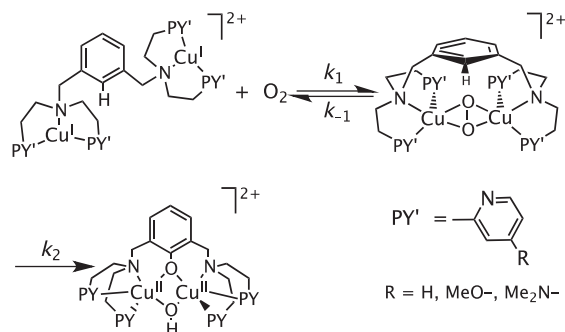
$[\text{Cu}^{\text{II}}_2(\text{MeOXYLO}^-)(\text{OH})](\text{PF}_6)_2$ ( <b>3c</b> )				$[\text{Cu}^{\text{I}}_2(\text{XYLO}^-)(\text{OH})](\text{PF}_6)_2$ ( <b>1c</b> )			
<i>Interatomic distances (Å)</i>							
Cu1–N1	2.054(8)	Cu1–N2	1.980(8)	Cu1–N1	2.034(14)	Cu1–N2	2.006(16)
Cu1–N3	2.180(8)	Cu2–N4	2.056(8)	Cu1–N3	2.258(13)	Cu2–N4	2.028(13)
Cu2–N5	2.190(8)	Cu2–N6	2.003(8)	Cu2–N5	2.149(15)	Cu2–N6	2.027(14)
Cu1–O1	1.969(6)	Cu1–O2	1.959(6)	Cu1–O1	1.979(10)	Cu1–O2	1.938(10)
Cu2–O1	1.987(6)	Cu2–O2	1.968(6)	Cu2–O1	1.972(11)	Cu2–O2	1.962(10)
<i>Interatomic angles (°)</i>							
O1–Cu1–O2	75.6(3)	O1–Cu1–N1	93.0(3)	O1–Cu1–O2	76.7(4)	O1–Cu1–N1	92.4(5)
O1–Cu1–N2	162.8(3)	O1–Cu1–N3	98.4(3)	O1–Cu1–N2	157.1(6)	O1–Cu1–N3	97.6(5)
O2–Cu1–N1	159.7(3)	O2–Cu1–N2	92.7(3)	O2–Cu1–N1	161.5(5)	O2–Cu1–N2	88.8(6)
O2–Cu1–N3	101.5(3)	N1–Cu1–N2	94.4(3)	O2–Cu1–N3	100.0(5)	N1–Cu1–N2	96.5(6)
N1–Cu1–N3	96.6(3)	N2–Cu1–N3	96.2(3)	N1–Cu1–N3	96.1(5)	N2–Cu1–N3	102.4(6)
O1–Cu2–O2	74.9(3)	O1–Cu2–N4	92.5(3)	O1–Cu2–O2	76.3(4)	O1–Cu2–N4	93.9(5)
O1–Cu2–N5	98.3(3)	O1–Cu2–N6	161.1(3)	O1–Cu2–N5	98.3(5)	O1–Cu2–N6	161.3(5)
O2–Cu2–N4	162.0(3)	O2–Cu2–N5	97.9(3)	O2–Cu2–N4	163.5(5)	O2–Cu2–N5	98.9(5)
O2–Cu2–N6	92.7(3)	N4–Cu2–N5	96.7(3)	O2–Cu2–N6	91.4(5)	N4–Cu2–N5	95.6(6)
N4–Cu2–N6	95.8(3)	N5–Cu2–N6	97.6(3)	N4–Cu2–N6	94.4(6)	N5–Cu2–N6	97.6(6)
Cu1–O1–Cu2	104.2(3)	Cu1–O2–Cu2	105.3(3)	Cu1–O1–Cu2	102.5(5)	Cu1–O2–Cu2	104.4(5)
Cu1–O1–C17	128.8(6)	Cu2–O1–C7	127.0(6)	Cu1–O1–C17	129.6(10)	Cu2–O1–C17	127.1(10)

**Fig. 4.** ORTEP diagram of the cationic portion of  $[\text{Cu}^{\text{II}}_2(\text{MeOXYLO})(\text{OH})]^{2+}$  (**3b**).

### 3.9. Stopped-flow kinetic studies

#### 3.9.1. Overall findings

As mentioned in the Section 1, detailed kinetics studies for the oxygenation reactions of  $[\text{Cu}^{\text{I}}(\text{R-XYL})]^{2+}$  (R on the central arene para to the position which is hydroxylated; R =  $-\text{NO}_2$ ,  $-\text{H}$ ,  $-\text{C}(\text{CH}_3)_3$ ,  $-\text{F}$ ) conform to Scheme 1, with the results providing corroborative evidence for a hydroxylation reaction mechanism involving an electrophilic peroxo species. Here, in our full investigation and kinetic analysis, we find that the reactions of the dicopper(I) complexes  $[\text{Cu}^{\text{I}}_2(\text{L})]^{2+}$  (**1b–d**, L =  $\text{MeOXYL}$ ,  $\text{Me}_2\text{NXYL}$  and UN, Fig. 1) with  $\text{O}_2$  in dichloromethane follow the same mechanism found for  $[\text{Cu}^{\text{I}}_2(\text{XYL})]^{2+}$  (**1a**) (Schemes 1 and 6). At low temperature,  $[\text{Cu}^{\text{I}}_2(\text{L})]^{2+}$  (**1a–d**, L =  $\text{XYL}$ ,  $\text{MeOXYL}$ ,  $\text{Me}_2\text{NXYL}$  and UN) binds dioxygen reversibly ( $k_1$ ,  $k_{-1}$ ) to form a  $\mu$ - $\eta^2$ : $\eta^2$ -(side-on) peroxo species  $[\text{Cu}^{\text{II}}_2(\text{L})(\text{O}_2^{2-})]^{2+}$  (**2a–d**), which subsequently hydroxylates the arene ( $k_2$ ) to give  $[\text{Cu}^{\text{II}}_2(\text{LO}^-)(\text{OH})]^{2+}$  (**3a–d**) products. Fig. 5 shows the UV–Vis behavior, when, for example,  $[\text{Cu}^{\text{I}}_2(\text{MeOXYL})]^{2+}$  (**1b**) reacts with excess  $\text{O}_2$  at  $-50^\circ\text{C}$ . Upon rapid mixing of solution of  $\text{O}_2$  and **1b**, there is very rapid formation of  $[\text{Cu}^{\text{II}}_2(\text{MeOXYL})(\text{O}_2^{2-})]^{2+}$

**Scheme 6.** Kinetic scheme deduced for the  $[\text{Cu}^{\text{I}}_2(\text{RXYL})]^{2+}$  (**1a–c**) oxygenation reactions employing  $\text{PY}'$  donor ligands.

(**2b**) with the predominant charge-transfer absorption at  $\lambda_{\text{max}} = 363\text{ nm}$  ( $\epsilon = 14000$ ) and the accompanying band  $437\text{ nm}$  ( $\epsilon = 2700$ ), past proven to be a species with the  $\mu$ - $\eta^2$ : $\eta^2$ -side-on peroxodicopper(II) core. In a unimolecular process **2b** subsequently decays and is transformed into  $[\text{Cu}^{\text{II}}_2(\text{MeOXYLO}^-)(\text{OH})]^{2+}$  with 370 and 650 nm absorptions. The inset of Fig. 5 shows the absorbance versus time trace at 363 nm, demonstrating a perfect correlation between experimental data and the suggested mechanism (Scheme 6).

It is found that at low temperature, the formation of the side-on peroxo species  $[\text{Cu}^{\text{II}}_2(\text{L})(\text{O}_2^{2-})]^{2+}$  (**2**) is complete, thus  $k_{-1}$  being irrelevant. However, at higher temperatures,  $k_{-1}$  has to be taken into account since the intermediate **2** is then only partially formed. Similar to the previously studied analogous systems [7,25], the hydroxylation step ( $k_2$ ) is composed of a thermal and of a photochemical temperature-independent term, and the latter dominates below  $\sim -40^\circ\text{C}$ . Thus, data acquired only at higher temperatures, where the photochemical terms could be accounted for and subtracted out, were used for determination of the activation parameters for  $k_2$ . An exceptional case was that for the oxygenation reaction of  $[\text{Cu}^{\text{I}}_2(\text{UN})](\text{PF}_6)_2$  (**1d**), where the photochemistry dominated in the whole temperature range (183–238 K) studied, initially precluding the determination of the thermal parameters of  $k_2$  for **1d**. The problem could be solved however, as discussed below.

The variable-temperature stopped-flow data of the oxygenation reactions of  $[\text{Cu}^{\text{I}}_2(\text{L})]^{2+}$  (**1a–d**, L =  $\text{HXYL}$ ,  $\text{MeOXYL}$ ,  $\text{Me}_2\text{NXYL}$  and UN) were analyzed by global analysis in the eigenvector space [23]

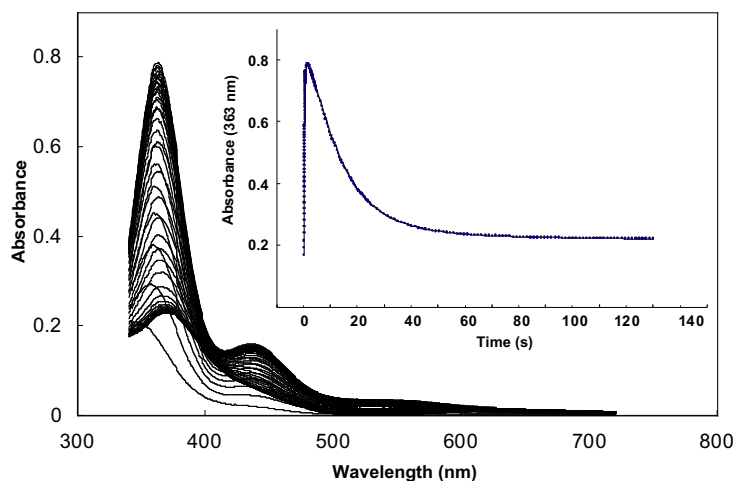


**Fig. 5.** Time-dependent UV-Vis spectra for the oxygenation of  $[\text{Cu}^{1/2}(\text{MeOXYL})]^{2+}$  (**1b**) at  $-50\text{ }^\circ\text{C}$ . Inset: absorbance vs. time at 363 nm; (x) experimental data; (—) calculated curve, based on the model described in Scheme 6. See text for further details.

**Table 4**  
Kinetic parameters for  $\text{O}_2$ -interactions with dicopper(I) complexes **1a–d**.

Parameters	$\text{HXYL}$ ( <b>1a</b> ) <sup>a</sup>	$\text{MeOXYL}$ ( <b>1b</b> )	$\text{Me}_2\text{NXYL}$ ( <b>1c</b> )	UN ( <b>1d</b> )
$k_1$ ( $\text{M}^{-1}\text{s}^{-1}$ )				
$\Delta H^\ddagger$ ( $\text{kJ mol}^{-1}$ )	$8.2 \pm 0.1$	$6.9 \pm 0.3$	$2.3 \pm 0.2$	$12.3 \pm 0.2$
$\Delta S^\ddagger$ ( $\text{J K}^{-1}\text{mol}^{-1}$ )	$-146 \pm 1$	$-149 \pm 1$	$-156 \pm 1$	$-132.4 \pm 0.8$
183 K	$385 \pm 5$	$(6.9 \pm 0.2) \times 10^2$	$(6.3 \pm 0.2) \times 10^3$	$(1.38 \pm 0.02) \times 10^2$
223 K	$(1.24 \pm 0.01) \times 10^3$	$(1.91 \pm 0.03) \times 10^3$	$(1.01 \pm 0.01) \times 10^4$	$(7.23 \pm 0.01) \times 10^2$
298 K	$(5.1 \pm 0.1) \times 10^3$	$(6.5 \pm 0.3) \times 10^3$	$(1.84 \pm 0.06) \times 10^4$	$(5.2 \pm 0.2) \times 10^3$
$k_{-1}$ ( $\text{s}^{-1}$ )				
$\Delta H^\ddagger$ ( $\text{kJ mol}^{-1}$ )	$70 \pm 1$	$78 \pm 1$	$71 \pm 2$	$67 \pm 1$
$\Delta S^\ddagger$ ( $\text{J K}^{-1}\text{mol}^{-1}$ )	$50 \pm 6$	$76 \pm 5$	$60 \pm 8$	$63 \pm 6$
183 K	$(1.5 \pm 0.4) \times 10^{-5}$	$(2.5 \pm 0.7) \times 10^{-6}$	$(3 \pm 1) \times 10^{-5}$	$(5.4 \pm 0.9) \times 10^{-4}$
223 K	$(7.20 \pm 0.05) \times 10^{-2}$	$(2.9 \pm 0.3) \times 10^{-2}$	$(1.3 \pm 0.2) \times 10^{-1}$	$1.79 \pm 0.1$
298 K	$(1.3 \pm 0.2) \times 10^3$	$(1.4 \pm 0.2) \times 10^3$	$(2.8 \pm 0.5) \times 10^3$	$(2.2 \pm 0.5) \times 10^4$
$k_2$ ( $\text{s}^{-1}$ )				
$\Delta H^\ddagger$ ( $\text{kJ mol}^{-1}$ )	$50 \pm 1$	$48.9 \pm 0.6$	$54 \pm 2$	$57 \pm 1^b$
$\Delta S^\ddagger$ ( $\text{J K}^{-1}\text{mol}^{-1}$ )	$-35 \pm 2$	$-47 \pm 2$	$-39 \pm 7$	$-26 \pm 6^b$
183 K	$(3.4 \pm 0.2) \times 10^{-4}$	$(1.5 \pm 0.2) \times 10^{-4}$	$(2.1 \pm 0.6) \times 10^{-5}$	$(1.1 \pm 0.2) \times 10^{-5}^b$
223 K	$(1.49 \pm 0.03) \times 10^{-1}$	$(6.0 \pm 0.2) \times 10^{-2}$	$(1.4 \pm 0.1) \times 10^{-2}$	$(1.04 \pm 0.06) \times 10^{-2}^b$
298 K	$172 \pm 8$	$61 \pm 3$	$26 \pm 4$	$31 \pm 8^b$

<sup>a</sup> Previously published results [7].

<sup>b</sup> Data obtained using single wavelength (361 nm) interrogation for the kinetic study.

and the kinetic and thermodynamic parameters deduced are listed in Tables 4 and 5. For the temperature-dependent reactions of interest ( $k_1$ ,  $k_{-1}$  and  $k_2$ ), plots of the kinetic and thermodynamic parameters  $\log(k/T)$  or  $\log(K/T)$  are all well behaved. Eyring plots of  $k_1$ ,  $k_{-1}$  and  $k_2$  for the  $\text{MeOXYL}$  complex are shown in Fig. 6.

### 3.9.2. Reversible $\text{O}_2$ -binding to the dicopper(I) complexes $[\text{Cu}^{1/2}(\text{L})]^{2+}$ (**1**)

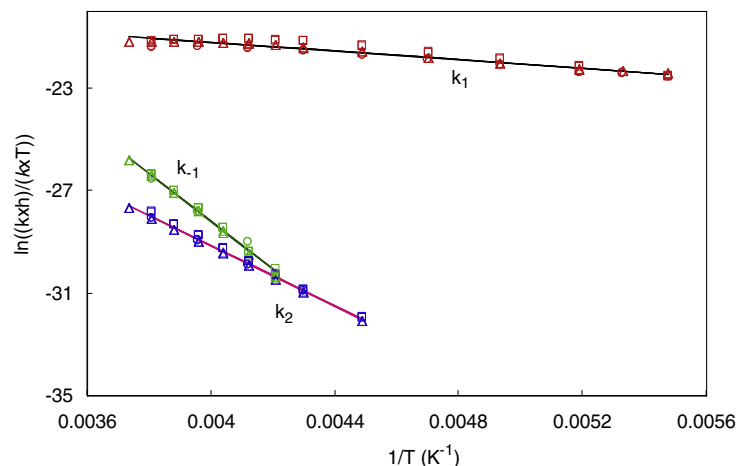
As seen from Table 4, the binding of  $\text{O}_2$  ( $k_1$ ) to the dicopper(I) complexes **1** to form the side-on peroxo species  $[\text{Cu}^{1/2}(\text{L})(\text{O}_2^{2-})]^{2+}$  (**2**) is characterized by very low activation enthalpies of less than  $12\text{ kJ mol}^{-1}$  and large compensating activation entropies of  $-136$  to  $-156\text{ J K}^{-1}\text{mol}^{-1}$ . Such observations may be rationalized on the basis of having reactive, easily oxidizable and coordinatively unsaturated (three coordinate) cuprous species. An additional reason for the observed low activation enthalpies may arise from the composite nature for the formation of the peroxodicopper(II) species  $[\text{Cu}^{1/2}(\text{L})]^{2+}$  (**2**) since it is unlikely that  $\text{O}_2$  would bind to both copper ions simultaneously. Rather, as described in previous studies, we suggest that the dioxygen first binds to one copper moiety to generate the superoxo intermediate (i.e.  $\text{Cu}^{\text{I}} \cdot \cdot \text{Cu}^{\text{II}}\text{-O}_2^-$ ) in a rapid, left-lying equilibrium and only in a second step forms the

spectroscopically detectable  $\mu$ -peroxo dicopper(II) moiety. Similar low or even negative activation enthalpies (i.e. consistent with a multi-step process) are observed for the formation of the peroxodicopper(II) complexes with a series of binucleating ligands Nn having the identical ligand set (i.e. the PY2 tridentate) linked instead by alkyl chains [26]. In addition, the formation of the  $\mu$ -1,2-(end-on)-peroxodicopper(II) complexes with a series of mononucleating tetradentate ligands exhibit negative activation enthalpies [12b,23,27] as a result of a similar pre-equilibrium step (formation of the initial  $\text{Cu}^{\text{I}}/\text{O}_2$  adduct, i.e. a superoxocopper(II) complex).

By contrast, Tolman, Zuberbühler and co-workers [9a,10a,28], through detailed stopped-flow kinetic studies, demonstrated that the formation of the  $\text{O}_2$ -adducts of mononuclear or binuclear copper(I) complexes containing substituted triazacyclononane (tacn) tridentate ligands is associated with considerable high activation enthalpies ( $\Delta H^\ddagger$  around  $40\text{ kJ mol}^{-1}$ ). These relatively large  $\Delta H^\ddagger$  values are comparable to those seen for the formation of  $\text{Cu}-\text{O}_2$  1:1 (i.e. superoxocopper(II) species) adducts in reactions of well-studied mononuclear copper(I) complexes with TMPA (=tris(2-pyridylmethyl)amine) and its analogs [12b,23]. Thus, it is concluded that the formation of superoxo intermediates, which are not spectroscopically observable in these tacn derivative cases, are the

**Table 5**  
Equilibrium parameters for O<sub>2</sub>-interaction with dicopper(I) complexes **1a–d**.

Parameters	<sup>H</sup> XYL ( <b>1a</b> )	<sup>MeO</sup> XYL ( <b>1b</b> )	<sup>Me<sup>2N</sup></sup> XYL ( <b>1c</b> )	UN ( <b>1d</b> )
$K_1$ ( $M^{-1}$ ) ( $=k_1/k_{-1}$ )				
$\Delta H^\circ$ ( $\text{kJ mol}^{-1}$ )	$-62 \pm 1$	$-71 \pm 2$	$-69 \pm 2$	$-55 \pm 1$
$\Delta S^\circ$ ( $\text{J K}^{-1} \text{mol}^{-1}$ )	$-196 \pm 6$	$-225 \pm 5$	$-222 \pm 9$	$-196 \pm 6$
183 K	$2.6 \times 10^7$	$(2.8 \pm 0.8) \times 10^8$	$(3 \pm 1) \times 10^8$	$(2.6 \pm 0.4) \times 10^5$
223 K	$1.7 \times 10^4$	$(6.6 \pm 0.6) \times 10^4$	$(7.5 \pm 0.8) \times 10^4$	$(4.0 \pm 0.1) \times 10^2$
298 K	3.9	$4.5 \pm 0.5$	$6 \pm 1$	$(2.4 \pm 0.5) \times 10^{-1}$

**Fig. 6.** Eyring plots for  $k_1$ ,  $k_{-1}$ , and  $k_2$  for  $[\text{Cu}_2^{\text{I}}(\text{MeOXYL})]^{2+}$  (**1b**);  $k$ , Boltzmann constant;  $h$ , Planck constant;  $[\text{O}_2] = 1.9 \times 10^{-3} \text{ M}$ ; **1b** ( $\Delta$ ),  $1.5 \times 10^{-4} \text{ M}$ ; ( $\circ$ ),  $3.0 \times 10^{-4} \text{ M}$ ; ( $\square$ ),  $4.1 \times 10^{-4} \text{ M}$ .

rate-determining steps in the oxygenation reactions of the corresponding copper(I) complexes. However, a stopped-flow kinetic study [12b] on the oxygenation reactions of a series of mononuclear copper(I) complexes with 4-pyridyl substituted TMPA ligands in propionitrile show that significant activation enthalpies (29–32  $\text{kJ mol}^{-1}$ ) associated with the formation of the superoxocopper(II) complexes involves the (rapid) dissociation of a coordinated nitrile in a strongly left-lying equilibrium. In addition, when weakly coordinating solvents such as tetrahydrofuran (THF) and acetone are used as solvents, much faster formation of superoxocopper(II) species are observed, demonstrating the importance of the solvent medium, where nitriles, which are excellent strong ligands for copper(I) centers [29], can compete with the O<sub>2</sub>-binding process.

More interestingly, for the oxygenation reactions of the dicopper(I) complexes  $[\text{Cu}_2^{\text{I}}(\text{RXYL})]^{2+}$  (**1a–c**), the rate of dioxygen binding ( $k_1$ ) increases (Table 4) as the ligand becomes more electron-donating (i.e. XYL to <sup>MeO</sup>XYL to <sup>Me<sup>2N</sup></sup>XYL), consistent with oxygenation being accompanied by electron transfer from copper(I) to O<sub>2</sub> (giving a superoxo or peroxy anion). The activation enthalpy  $\Delta H^\ddagger$  for  $k_1$  also exhibits a trend, where  $\Delta H^\ddagger$  decreases as the ligand electron-donating ability increases, again suggesting more favorable dioxygen binding with strong electron-donating ligands. Presumed ligand constraints (as seen in X-ray structure of  $[\text{Cu}_2^{\text{II}}(\text{UN}-\text{O}^-)(-\text{OH})]^{2+}$  (**3d**), discussed above) are also shown to affect Cu<sub>2</sub>-O<sub>2</sub> binding, where a slower dioxygen binding (i.e. smaller  $k_1$ ) and a higher activation enthalpy  $\Delta H^\ddagger$  (for  $k_1$ ) are observed for the copper(I) complex  $[\text{Cu}_2^{\text{I}}(\text{UN})]^{2+}$  (**1d**) with the unsymmetrical ligand UN (Fig. 1), compared to that for the parent ligand XYL (Table 4). The observed differences suggest that for these binuclear copper(I)-complexes, the formation of the superoxo intermediates (i.e. initial O<sub>2</sub>-adduct) is unlikely to be the rate-determining step since it is hard to conceive that individual

copper(I) centers with nearly identical coordination environments (UN versus XYL) would exhibit different intrinsic reactivity toward O<sub>2</sub> (for the formation of superoxo intermediates), again manifesting the composite nature of these oxygenation reactions.

In contrast to the observed very low activation enthalpies (<12  $\text{kJ mol}^{-1}$ ) for  $k_1$ , large activation enthalpies  $\Delta H^\ddagger$  (67–78  $\text{kJ mol}^{-1}$ ) along with positive activation entropies are associated with the dissociation ( $k_{-1}$ ) of O<sub>2</sub> from Cu<sub>2</sub>O<sub>2</sub> complexes. Although not dramatic effects, a larger rate constant  $k_{-1}$ , as well as a lower activation enthalpy (associated with  $k_{-1}$ ) are observed for the UN complex compared to that for XYL complexes (Table 4), suggesting that ligand constraints in  $[\text{Cu}_2^{\text{II}}(\text{UN})(\text{O}_2^{2-})]^{2+}$  (**2d**) decreases its copper–dioxygen bonding strength,  $k_{-1}$ , representing the breaking of a Cu–O bond and release of O<sub>2</sub>. However, no direct correlation between the ligand electron-donating ability and the copper–dioxygen binding strength ( $\Delta H^\ddagger$  for  $k_{-1}$ , Table 4) is observed. In fact, the <sup>MeO</sup>XYL complex exhibits a higher activation enthalpy  $k_{-1}$  compared to that for the parent XYL ligand, which is in line with the notion that electron-donating ligand somehow increases the Cu–O bond strength in the peroxy complex **2**. Perhaps Cu(II) → O (peroxide) back-bonding is not insignificant in  $[\text{Cu}_2^{\text{II}}(\text{L})(\text{O}_2^{2-})]^{2+}$  (**2**) complex, as has been discussed with respect to the electronic structure and bonding in  $\mu\text{-}\eta^2\text{:}\eta^2\text{-}(\text{side-on})\text{-peroxodicopper(II)}$  species [30]. Nevertheless,  $\Delta H^\ddagger$  and  $k_{-1}$  values are almost identical for the <sup>Me<sup>2N</sup></sup>XYL (most electron-donating ligand) and <sup>H</sup>XYL complexes, exhibiting no effect of a more electron-donating ligand (<sup>Me<sup>2N</sup></sup>XYL). As mentioned, it was proposed that there is some interaction between the dicopper-bound electrophilic peroxy group and the xylyl  $\pi$  systems in  $[\text{Cu}_2^{\text{II}}(\text{L})(\text{O}_2^{2-})]^{2+}$  (**2**) due to their close proximity. Perhaps this can provide an explanation for the absence of a correlation between the copper–dioxygen bond strength in the peroxy complex **2** and the ligand electronic-donating ability.

From  $k_1$  and  $k_{-1}$ , equilibrium constants  $K_1 = k_1/k_{-1}$  and the corresponding thermodynamic parameters  $\Delta H^\circ$  and  $\Delta S^\circ$  can be calculated; they are collected in Table 5. Here, again, the thermostability ( $\Delta H^\circ$ ) of the peroxy complex  $[\text{Cu}^{\text{II}}_2(\text{L})(\text{O}_2^{2-})]^{2+}$  (**2**) appears to correlate with the effect of ligand constraints, where the unsymmetrical ligand UN affords a less stable peroxy complex compared to that with XYL ligand, reflected by their  $K_1$  and  $\Delta H^\circ$  values. Ligand constraints or steric hindrance have well been demonstrated to influence the stability of copper–dioxygen adducts formed [27,31]. A complex possessing a binucleating analogue (DO, Fig. 7) of TMPA with  $-\text{CH}_2\text{OCH}_2-$  linked pyridyl groups exhibits significant stability in acetone and in fact, the thermodynamic parameters could not be obtained (i.e. since its formation is essentially complete at all temperatures) [31a]. By contrast, an analogous ligand ( $\text{D}^1$ , Fig. 7) with  $-\text{CH}_2\text{CH}_2-$  linker leads to a strained and much less stable dioxygen adduct. In addition, in the oxygenation reactions of a series of binuclear copper(I)-complexes (Nn, Fig. 7) containing the same tridentate PY2 units [26], the length of the alkyl chain (i.e.  $-(\text{CH}_2)_n-$ ) connecting the two PY2 units appears to have a remarkable effect on the equilibrium constants  $K_1$  for the formation of the  $\mu-\eta^2:\eta^2$ -peroxodicopper(II) complexes  $[\text{Cu}^{\text{I}}(\text{Nn})(\text{O}_2^{2-})]^{2+}$ . The  $[\text{Cu}^{\text{I}}_2(\text{N5})]^{2+}$  complex with the longest alkyl linker ( $-(\text{CH}_2)_5-$ ) affords the largest  $K_1$  value (i.e. most stable peroxy complex), which is in accord with the view that the N5 complex forms the most favorable  $\text{Cu}_2\text{O}_2$  structure due to the relatively unconstrained nature of the ligand. This is consistent with a resonance Raman study [32] of  $\text{Cu}_2\text{O}_2$  complexes with Nn ligands, where the N5 complex exhibits the lowest  $\nu(\text{O}-\text{O})$  value (due to enhance back donation from Cu to the peroxy  $\sigma^*$  orbital within the planar  $\text{Cu}_2\text{O}_2$  core), closest to that for the unconstrained mononuclear Cu-MePY2 complex,  $[\{\text{Cu}^{\text{I}}(\text{MePY2})\}_2(\mu-\eta^2:\eta^2-\text{O}_2^{2-})]^{2+}$ . Comparing to these Nn ligands, the  $^{\text{R}}\text{XYL}$  and UN ligands are more constrained because of the bulky and less flexible xyllyl groups connecting the PY2 tridentate moieties. Thus, the overall reaction enthalpies  $\Delta H^\circ$  for the XYL and UN systems are considerably less negative than those with Nn ligands,  $-56 \text{ kJ mol}^{-1}$  for UN,  $-62$  to  $-71 \text{ kJ mol}^{-1}$  for  $^{\text{R}}\text{XYL}$ ,  $-81$  to  $-84 \text{ kJ mol}^{-1}$  for Nn, all forming dicopper complexes with the  $[\text{Cu}^{\text{II}}_2(\mu-\eta^2:\eta^2-\text{O}_2^{2-})]^{2+}$  core.

The substituted XYL ligands ( $^{\text{MeO}}\text{XYL}$  and  $^{\text{Me}_2\text{N}}\text{XYL}$ ) afford more stable peroxy complexes compared to that with the parent XYL ligand (i.e. more negative  $\Delta H^\circ$  and bigger  $K_1$ , Table 5). However, the peroxy complexes with  $^{\text{MeO}}\text{XYL}$  and  $^{\text{Me}_2\text{N}}\text{XYL}$  ligands exhibit nearly identical thermostabilities (Table 5), again reflecting no direct correlation between the stability of the peroxy species **2** and the ligand electron-donating ability, as said before possibly due to interaction between the peroxy core and  $\pi$  orbitals of xyllyl linker group.

In summary, the thermodynamic parameters ( $\Delta H^\circ$  and  $\Delta S^\circ$ ) clearly indicate that the dioxygen binding to these dicopper(I) complexes  $[\text{Cu}^{\text{I}}_2(\text{L})]^{2+}$  (**1**) is entirely driven by enthalpy, while large negative entropies result in their room-temperature instability. Ligand constraints are shown to have a significant effect on the dioxygen binding ( $k_1$ ) as well as the stability ( $K_1$ ,  $\Delta H^\circ$ ) of the resulting

peroxy species  $[\text{Cu}^{\text{II}}_2(\text{L})(\text{O}_2^{2-})]^{2+}$  (**2**). Ligand electron-donating ability appears to affect the binding of dioxygen ( $k_1$  and  $\Delta H^\circ$  for  $k_1$ ) to the copper(I) complexes, where more electron-donating ligands favor  $\text{O}_2$ -binding with smaller activation enthalpies. However, no direct correlation between the stability of the resulting peroxy complexes **2** with ligand electronic properties are observed, possibly due to some interaction between the  $\text{Cu}_2\text{O}_2$  core and xyllyl  $\pi$  orbitals (as previously mentioned).

### 3.9.3. Arene hydroxylation step $k_2$

As shown in Fig. 5,  $[\text{Cu}^{\text{II}}_2(\text{MeOXYL})(\text{O}_2^{2-})]^{2+}$  (**2b**) as well as the other side-on peroxy species  $[\text{Cu}^{\text{II}}_2(\text{L})(\text{O}_2^{2-})]^{2+}$  (**2**) are not stable (except the UN complex **2d**, *vide infra*) even at low temperature, as reflected by the disappearance of their UV–Vis features, and their subsequent decay leads to arene hydroxylation (Schemes 1 and 6). However, bench-top observations mentioned above clearly indicate that complex **2d** is much more stable (i.e. longer-lived by bench-top UV–Vis monitoring) than the other peroxy complexes with XYL or substituted XYL ligands ( $^{\text{MeO}}\text{XYL}$  and  $^{\text{Me}_2\text{N}}\text{XYL}$ ). This suggests that subsequent hydroxylation reaction is less favorable with the UN ligand, which possesses an unsymmetrical and strained ligand environment. A nearly ideal orientation of the arene substrate and the peroxy core in  $[\text{Cu}^{\text{II}}_2(\text{R-XYL})(\text{O}_2^{2-})]^{2+}$  complexes (Schemes 1 and 6) are proposed for these facile hydroxylation reactions [6b,27]. Thus, possible disruption of this desirable orientation caused by ligand constraints of the unsymmetrical UN ligand inhibits the occurrence of a fast arene hydroxylation reaction which otherwise might be expected for **2d** at low temperature ( $<193 \text{ K}$ ). However, at higher temperatures, **2d** is not stable and it does decay, leading to the formation of the well-characterized hydroxylation product  $[\text{Cu}^{\text{II}}_2(\text{UN}-\text{O})(-\text{OH})]^{2+}$  (**3d**) [16].

As mentioned, the experimental methods used for most of the kinetic studies leads to dominating photochemistry relating to the hydroxylation step ( $k_2$ ) for  $[\text{Cu}^{\text{II}}_2(\text{UN})(\text{O}_2^{2-})]^{2+}$  (**2d**); the diode array spectrometer inputs rather intense light over the whole spectral region. As copper–dioxygen complexes in general possess very strong peroxy-to-Cu(II) charge-transfer absorptions, it is not too surprising that photochemical reactions would exist. In fact, metal–dioxygen complex photochemistry in general has and does attract general interest [33], and  $\text{Cu}_n(\text{O}_2)]^{n+}$  complexes are candidates for future studies. We found that the way around the photochemistry issue for the UN system was to go to single-wavelength studies. Thus, Fig. 8 shows data obtained via 361 nm monitoring of the  $[\text{Cu}^{\text{I}}_2(\text{UN})]^{2+}$  (**1d**) +  $\text{O}_2$  reaction. From such data, valid kinetic parameters were obtained for  $k_2$  (Table 4). Fig. 9 shows an Eyring plot for  $k_2$  avoiding photochemistry and a comparison to the data obtained when using the diode array spectrometer.

In line with the benchtop spectroscopic findings for  $[\text{Cu}^{\text{I}}_2(\text{UN})]^{2+}$  (**1d**) oxygenation mentioned above, the  $k_2$  kinetic parameters reveal that indeed, the rate of the arene hydroxylation reaction,  $[\text{Cu}^{\text{II}}_2(\text{UN})(\text{O}_2^{2-})]^{2+}$  (**2d**)  $\rightarrow$   $[\text{Cu}^{\text{II}}_2(\text{UNO})(-\text{OH})]^{2+}$  (**3d**), is less than

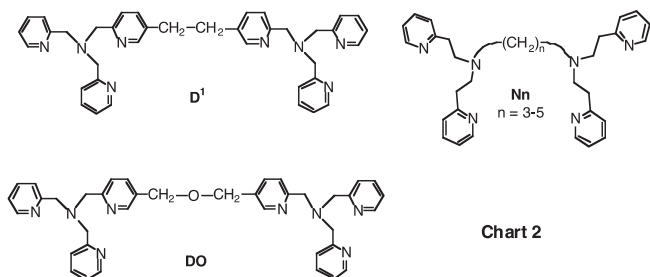


Fig. 7. Dinucleating ligands used in other  $\text{Cu}^{\text{I}}_2/\text{O}_2$  kinetic studies.

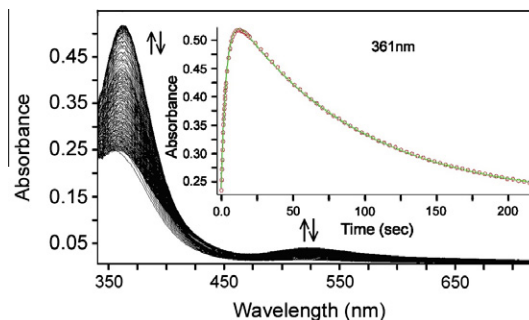


Fig. 8. Time-dependent spectra and 361 nm monitoring of the  $[\text{Cu}^{\text{I}}_2(\text{UN})]^{2+}$  (**1d**) +  $\text{O}_2$  reaction in  $\text{CH}_2\text{Cl}_2$  at 183 K.

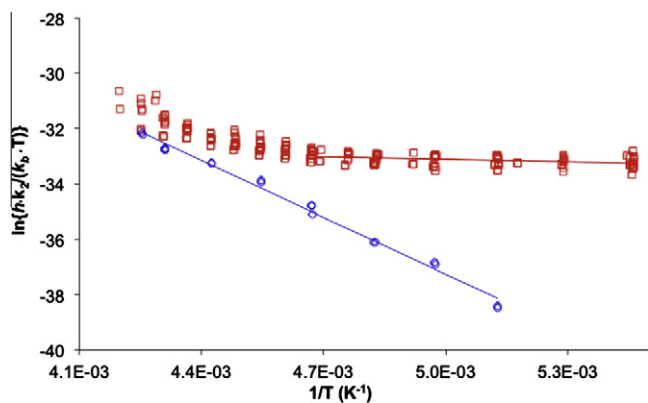


Fig. 9. Eyring plots on data obtained for the hydroxylation reaction ( $k_2$ ) of  $[\text{Cu}^{\text{II}}_2(\text{UN})(\text{O}_2^{2-})]^{2+}$  (**2d**) using either the diode array spectrometer (red) or single wavelength monitoring (blue; lower straight line). (For interpretation of the references to color in this figure legend, the reader is referred to the web version of this article.)

is found for the other  $^{\text{R}}\text{XYL}$  dicopper complex analogues. This especially obvious if one compares  $k_2$  values and corresponding activation parameters with the hydroxylation reaction for the parent complex  $[\text{Cu}^{\text{II}}_2(^{\text{H}}\text{XYL})(\text{O}_2^{2-})]^{2+}$  (Table 4). For example, at 223 K,  $k_2$  is 15 times smaller for the UN system. While not a huge difference, it is clearly sufficient to have allowed facile bench-top UV–Vis spectroscopic monitoring of **2d** at 183 K (*vide supra*) [16], while  $[\text{Cu}^{\text{II}}_2(^{\text{H}}\text{XYL})(\text{O}_2^{2-})]^{2+}$  (**2a**) cannot be detected. As discussed, the slowed arene hydroxylation rate for  $[\text{Cu}^{\text{II}}_2(\text{UN})(\text{O}_2^{2-})]^{2+}$  (**2d**) undoubtedly reflects a less than ideal proximity or orientation of the complex's electrophilic peroxy group toward the arene  $\pi$ -system.

Ligand substituents also affect the arene hydroxylation reactions of the peroxy complexes  $[\text{Cu}^{\text{II}}_2(\text{L})(\text{O}_2^{2-})]^{2+}$  (**2**). As seen in Table 4,  $k_2$  decreases with increasing ligand electron-donating ability. This is consistent with the proposed reaction mechanism involving an electrophilic peroxy group. Strong electron-donating groups provide more electron density to the peroxy core through bonding to the copper centers, which should disfavor the electrophilic attack of the peroxy species. The enhanced electrophilic nature of a  $\mu$ - $\eta^2$ : $\eta^2$ -peroxy group relative to an end-on peroxy-dicopper(II) structure (see Scheme 2) is supported by theoretical studies [30,34], where the peroxide has two antibonding interactions with each of the two copper ions, resulting in a much less negative peroxide due to extremely large  $\sigma$ -donor interactions between peroxide and copper. The electrophilic behavior of the side-on peroxy moiety has also been demonstrated in a detailed study comparing reactivity patterns of the side-on versus end-on peroxy dicopper(II) species [35]. However, theoretical calculations on the electronic structure of side-on peroxodicopper(II) moieties show that the bonding interaction between the  $\text{Cu } d_{x^2-y^2}$  orbitals and the  $\text{O}_2^{2-} \sigma^*$  orbital facilitate the back-donation of electron-density which is responsible for the weak  $\nu(\text{O}-\text{O})$  stretch ( $\sim 740 \text{ cm}^{-1}$ ) in side-on peroxodicopper(II) species compared to the end-on analogues ( $\sim 820 \text{ cm}^{-1}$ ).

In summary, the proposed reaction mechanism for the endogenous arene hydroxylation reaction effected by the side-on peroxy complexes with  $\text{XYL}$  and related ligands are further confirmed by the kinetic/thermodynamic studies described here. Strong electron-donating ligands afford the formation of more electron-rich peroxy moieties, which disfavor their electrophilic arene hydroxylation (i.e. smaller rate constants  $k_2$  Scheme 1). Ligand constraints in the unsymmetrical UN ligand results in a significantly slower hydroxylation due to the disruption of the ideal orientation of

the peroxy core and arene substrate present in the symmetrical ligand systems.

#### 4. Conclusions

The effect of ligand electronic variations on the dioxygen binding and the arene hydroxylation reactions of the resulting  $\text{Cu}_2\text{O}_2$  species has been achieved by incorporating 4-pyridyl substituents in the extensively studied  $\text{XYL}$  system. The detailed kinetic/thermodynamic studies of the oxygenation reactions of the corresponding copper(I) complexes with substituted  $\text{XYL}$  ligands reveal that the more electron-donating ligand favors  $\text{O}_2$ -binding to form the peroxodicopper(II) complexes  $[\text{Cu}^{\text{II}}_2(\text{L})(\text{O}_2^{2-})]^{2+}$  (**2**). However, no direct correlation between the ligand electron-donating ability and the stability of the peroxy complexes is observed, which is rationalized by some interaction between the  $\text{Cu}_2\text{O}_2$  core and the xylyl  $\pi$ -orbitals. Less favorable arene hydroxylation of the peroxy complexes with strong electron-donating ligands is consistent with the proposed reaction mechanism involving electrophilic attack of the peroxy moiety on the xylyl ring.

Ligand structural effects are also investigated utilizing the analogous but unsymmetrical UN ligand. The kinetic and thermodynamic data show that the ligand constraints have significant effect on the formation, stability and reactivity of the peroxy complex. A significantly slower thermal arene hydroxylation reaction is observed for the UN complex compared with the  $\text{XYL}$  complex, suggesting disruption of the ideal positioning of the peroxy core towards the arene substrate.

The present detailed systematic investigations provide a wealth of new chemistry and information concerning how ligand electronic and structural elements affect copper–dioxygen interactions as well as C–H activation, i.e. biomimetic hydroxylation mediated by copper–dioxygen chemistry. Such fundamental studies help to unravel the detailed nature of copper–dioxygen reactivity and provide a basis for a deeper understanding of relevant biological systems as well as potential practical applications for copper mediated oxidative chemistry.

#### Acknowledgments

The authors acknowledge the research support from the USA National Institutes of Health Grant GM28962 (K.D.K.) and the Swiss National Science Foundation (A.D.Z.).

#### Appendix A. Supplementary material

CCDC 867041 contains the supplementary crystallographic data for complex  $[\text{Cu}^{\text{II}}_2(\text{MeOXYLO})(\text{OH})(\text{PF}_6)_2]$  (**3b**). These data can be obtained free of charge from The Cambridge Crystallographic Data Centre via [www.ccdc.cam.ac.uk/data\\_request/cif](http://www.ccdc.cam.ac.uk/data_request/cif). Supplementary data associated with this article can be found, in the online version, at doi:10.1016/j.ica.2012.01.042.

#### References

- (a) E.I. Solomon, J.W. Ginsbach, D.E. Heppner, M.T. Kieber-Emmons, C.H. Kjaergaard, P.J. Smeets, L. Tian, J.S. Woertink, *Faraday Discuss.* 148 (2011) 11; (b) E.I. Solomon, P. Chen, M. Metz, S.-K. Lee, A.E. Palmer, *Angew. Chem., Int. Ed.* 40 (2001) 4570; (c) R.A. Himes, K.D. Karlin, *Curr. Opin. Chem. Biol.* 13 (2009) 119; (d) L.M. Mirica, X. Ottenwaelder, T.D.P. Stack, *Chem. Rev.* 104 (2004) 1013; (e) E.A. Lewis, W.B. Tolman, *Chem. Rev.* 104 (2004) 1047; (f) L.Q. Hatcher, K.D. Karlin, *J. Biol. Inorg. Chem.* 9 (2004) 669.
- K.A. Magnus, B. Hazes, H. Ton-That, C. Bonaventura, J. Bonaventura, W.G.J. Hol, *Proteins Struct. Funct. Genet.* 19 (1994) 302.
- (a) E.I. Solomon, U.M. Sundaram, T.E. Machonkin, *Chem. Rev.* 96 (1996) 2563; (b) S. Itoh, S. Fukuzumi, *Acc. Chem. Res.* 40 (2007) 592.
- (a) J.P. Klinman, *J. Biol. Chem.* 281 (2006) 3013; (b) J.P. Klinman, *Chem. Rev.* 96 (1996) 2541.

- [5] (a) R. Balasubramanian, S.M. Smith, S. Rawat, L.A. Yatsunyk, T.L. Stemmler, A.C. Rosenzweig, *Nature* 465 (2010) 115;  
(b) R. Himes, K. Barnese, K. Karlin, *Angew. Chem., Int. Ed.* 49 (2010) 6714.
- [6] (a) K.D. Karlin, Y. Gultneh, J.C. Hayes, R.W. Cruse, J.W. McKown, J.P. Hutchinson, J. Zubieta, *J. Am. Chem. Soc.* 106 (1984) 2121;  
(b) E. Pidcock, H.V. Obias, C.X. Zhang, K.D. Karlin, E.I. Solomon, *J. Am. Chem. Soc.* 120 (1998) 7841;  
(c) K.D. Karlin, A.D. Zuberbühler, in: J. Reedijk, E. Bouwman (Eds.), *Bioinorganic Catalysis*, Second Edition, Revised and Expanded, Marcel Dekker, Inc., New York, 1999, pp. 469–534.
- [7] K.D. Karlin, M.S. Nasir, B.I. Cohen, R.W. Cruse, S. Kaderli, A.D. Zuberbühler, *J. Am. Chem. Soc.* 116 (1994) 1324.
- [8] M.S. Nasir, B.I. Cohen, K.D. Karlin, *J. Am. Chem. Soc.* 114 (1992) 2482.
- [9] (a) S. Mahapatra, S. Kaderli, A. Llobet, Y.-M. Neuhold, T. Palanché, J.A. Halfen, V.G. Young Jr., T.A. Kaden, L. Que Jr., A.D. Zuberbühler, W.B. Tolman, *Inorg. Chem.* 36 (1997) 6343;  
(b) P.L. Holland, K.R. Rodgers, W.B. Tolman, *Angew. Chem., Int. Ed.* 38 (1999) 1139;  
(c) A.H. Ole Sander, Christian Näther, Christian Würtele, Max C. Holthausen, Siegfried Schindler, Felix Tuczek, *Chem. Eur. J.* 14 (2008) 9714;  
(d) R. Menif, A.E. Martell, P.J. Squattrito, A. Clearfield, *Inorg. Chem.* 29 (1990) 4723.
- [10] (a) J.A. Halfen, S. Mahapatra, E.C. Wilkinson, S. Kaderli, V.G. Young Jr., L. Que Jr., A.D. Zuberbühler, W.B. Tolman, *Science* 271 (1996) 1397;  
(b) B.T. Op't Holt, M.A. Vance, L.M. Mirica, D.E. Heppner, T.D.P. Stack, E.I. Solomon, *J. Am. Chem. Soc.* 131 (2009) 6421.
- [11] L.M. Mirica, M. Vance, D.J. Rudd, B. Hedman, K.O. Hodgson, E.I. Solomon, T.D.P. Stack, *Science* 308 (2005) 1890.
- [12] (a) M.J. Henson, M.A. Vance, C.X. Zhang, H.-C. Liang, K.D. Karlin, E.I. Solomon, *J. Am. Chem. Soc.* 125 (2003) 5186;  
(b) C.X. Zhang, S. Kaderli, M. Costas, E.-i. Kim, Y.-M. Neuhold, K.D. Karlin, A.D. Zuberbühler, *Inorg. Chem.* 42 (2003) 1807;  
(c) C.X. Zhang, H.-C. Liang, E.-i. Kim, J. Shearer, M.E. Helton, E. Kim, S. Kaderli, C.D. Incarvito, A.D. Zuberbühler, A.L. Rheingold, K.D. Karlin, *J. Am. Chem. Soc.* 125 (2003) 634;  
(d) J. Shearer, C.X. Zhang, L.N. Zakharov, A.L. Rheingold, K.D. Karlin, *J. Am. Chem. Soc.* 127 (2005) 5469.
- [13] (a) D.F. Evans, *J. Chem. Soc.* (1959) 2003;  
(b) D.H. Live, S.I. Chan, *Anal. Chem.* 42 (1970) 791.
- [14] (a) K.D. Karlin, R.W. Cruse, Y. Gultneh, A. Farooq, J.C. Hayes, J. Zubieta, *J. Am. Chem. Soc.* 109 (1987) 2668;  
(b) K.D. Karlin, M.S. Haka, R.W. Cruse, G.J. Meyer, A. Farooq, Y. Gultneh, J.C. Hayes, J. Zubieta, *J. Am. Chem. Soc.* 110 (1988) 1196.
- [15] L.Q. Hatcher, M.A. Vance, A.A. Narducci Sarjeant, E.I. Solomon, K.D. Karlin, *Inorg. Chem.* 45 (2006) 3004.
- [16] M.S. Nasir, K.D. Karlin, D. McGowty, J. Zubieta, *J. Am. Chem. Soc.* 113 (1991) 698.
- [17] (a) J.V. Dagdigian, V. McKee, C.A. Reed, *Inorg. Chem.* 21 (1982) 1332;  
(b) M. Munakata, M. Maekawa, S. Kitagawa, S. Matsuyama, H. Masuda, *Inorg. Chem.* 28 (1989) 4300.
- [18] I. Sanyal, K.D. Karlin, R.W. Strange, N.J. Blackburn, *J. Am. Chem. Soc.* 115 (1993) 11259.
- [19] T.N. Sorrell, M.R. Malachowski, D.L. Jameson, *Inorg. Chem.* 21 (1982) 3250.
- [20] K.D. Karlin, Z. Tyeklár, A. Farooq, M.S. Haka, P. Ghosh, R.W. Cruse, Y. Gultneh, J.C. Hayes, P.J. Toscano, J. Zubieta, *Inorg. Chem.* 31 (1992) 1436.
- [21] M. Ciampolini, L. Fabbri, A. Perotti, A. Poggi, B. Seghi, F. Zanobini, *Inorg. Chem.* 26 (1987) 3527.
- [22] I. Sanyal, M. Mahroof-Tahir, S. Nasir, P. Ghosh, B.I. Cohen, Y. Gultneh, R. Cruse, A. Farooq, K.D. Karlin, S. Liu, J. Zubieta, *Inorg. Chem.* 31 (1992) 4322.
- [23] K.D. Karlin, N. Wei, B. Jung, S. Kaderli, P. Niklaus, A.D. Zuberbühler, *J. Am. Chem. Soc.* 115 (1993) 9506.
- [24] K.D. Karlin, A. Farooq, J.C. Hayes, B.I. Cohen, T.M. Rowe, E. Sinn, J. Zubieta, *Inorg. Chem.* 26 (1987) 1271.
- [25] R.W. Cruse, S. Kaderli, K.D. Karlin, A.D. Zuberbühler, *J. Am. Chem. Soc.* 110 (1988) 6882.
- [26] H.-C. Liang, K.D. Karlin, R. Dyson, S. Kaderli, B. Jung, A.D. Zuberbühler, *Inorg. Chem.* 39 (2000) 5884.
- [27] K.D. Karlin, S. Kaderli, A.D. Zuberbühler, *Acc. Chem. Res.* 30 (1997) 139.
- [28] S. Mahapatra, V.G. Young Jr., S. Kaderli, A.D. Zuberbühler, W.B. Tolman, *Angew. Chem., Int. Ed. Engl.* 36 (1997) 130.
- [29] (a) F.H. Jardine, *Adv. Inorg. Chem. Radiochem.* 17 (1975) 115;  
(b) B.J. Hathaway, in: G. Wilkinson (Ed.), *Comprehensive Coordination Chemistry*, vol. 5, Pergamon, New York, 1987, pp. 533–774.
- [30] P.K. Ross, E.I. Solomon, *J. Am. Chem. Soc.* 113 (1991) 3246.
- [31] (a) K.D. Karlin, D.-H. Lee, S. Kaderli, A.D. Zuberbühler, *Chem. Commun.* (1997) 475;  
(b) D.-H. Lee, N. Wei, N.N. Murthy, Z. Tyeklár, K.D. Karlin, S. Kaderli, B. Jung, A.D. Zuberbühler, *J. Am. Chem. Soc.* 117 (1995) 12498.
- [32] E. Pidcock, H.V. Obias, M. Abe, H.-C. Liang, K.D. Karlin, E.I. Solomon, *J. Am. Chem. Soc.* 121 (1999) 1299.
- [33] D.M. Wagnerová, K. Lang, *Coord. Chem. Rev.* 255 (2011) 2904.
- [34] E.I. Solomon, F. Tuczek, D.E. Root, C.A. Brown, *Chem. Rev.* 94 (1994) 827.
- [35] P.P. Paul, Z. Tyeklár, R.R. Jacobson, K.D. Karlin, *J. Am. Chem. Soc.* 113 (1991) 5322.